EUROPEAN ORGANIZATION FOR NUCLEAR RESEARCH

CERN-EP/79-56
13 June 1979

STUDIES OF PROTON-PROTON COLLISIONS AT THE CERN ISR WITH AN IDENTIFIED CHARGED HADRON OF HIGH TRANSVERSE MOMENTUM AT 90°

III. JET-LIKE STRUCTURES

M.G. Albrow[1], S. Almehed[2], P.S.L. Booth[3], X. de Bouard[4], H. Bøggild[5], L.J. Carroll[3], P. Catz[4], E. Dahl-Jensen[5], I. Dahl-Jensen[5], G. Damgaard[5], G. von Dardel[2], N. Elverhaug[6], K.H. Hansen[5], J.N. Jackson[3], G. Jancso[4+], G. Jarlskog[2], H.B. Jensen[5], L. Jönsson[2], A. Klovning[6], E. Lillethun[6], A. Lu[4], B. Lörstad[2], N.A. McCubbin[1], A. Melin[2], H.E. Miettinen[5$], R. Møller[5], B.S. Nielsen[5x], S.Ø. Nielsen[5], J.O. Petersen[5x], J.A.J. Skard[6], P. Villeneuve[7].

British-French-Scandinavian Collaboration

1) Rutherford Laboratory, Chilton, Didcot, United Kingdom
2) University of Lund, Sweden
3) University of Liverpool, United Kingdom
4) Laboratoire d'Annecy-le-Vieux de Physique des Particules, Annecy, France
5) Niels Bohr Institute, Copenhagen, Denmark
6) University of Bergen, Norway
7) LPNHE, University of Paris VI, Paris, France

Geneva - May 1979
(Submitted to Nuclear Physics B)

+) Now at the Central Research Institute for Physics, Hungarian Academy of Sciences, Budapest.
x) Now at CERN, Geneva.
$) Now at Rice University, Houston, Texas.

ABSTRACT

Results are reported from a study of proton-proton collisions at a c.m. energy of 52.6 GeV, in which a charged hadron with large transverse momentum is emitted near 90^{o} in the c.m.s. Pairs of particles opposite in azimuth to the trigger particle with transverse momenta above a fixed value show evidence for jet-like structures. Methods to isolate jet-like groups of particles are compared on the basis of a simple model of jet events. Results on the distribution and internal properties of jets from proton-proton collisions are presented, using one of these methods. The jets are found to be very similar in structure to jets observed in $e^{+}e^{-}$ annihilations and in νp scattering, but have about 20% higher multiplicity mainly originating at small $x_{\parallel}$. The charge of the jets is correlated with the charge of the trigger particle.

1. INTRODUCTION

The concept of hadronic jets, although still somewhat loosely defined, has gained considerable importance in the study of high energy collisions with large momentum transfers involving hadrons in the final state. For recent comprehensive treatments of the field, see (1,2).

Generalizing from low transverse momentum hadron-hadron collisions, a jet can be defined to be a set of hadrons with a large total momentum and with limited momentum components transverse to the direction of this total momentum.

Jet-like structures have been observed in the final states of e^+e^- annihilation (3,16), deep inelastic lepton nucleon scattering (4), and at large transverse momentum, p_T, in hadron-hadron collisions (5-8,10). The bulk of particles produced in hadron-hadron collisions at low transverse momentum, with exponentially damped p_T-distributions, can also be said to form jets in the directions of the colliding particles. It is still an open question what similarities or differences exist between the jets produced in the various types of collisions.

In this experiment we have studied proton-proton collisions in which a charged hadron (the trigger particle) is produced near 90° in the c.m.s. The subject of this paper is an investigation of jet-like structures among the many charged particles emitted in these collisions. In previous publications (9,10) (hereafter referred to as papers I and II), we have presented results on the correlation between the high p_T trigger particle and the forward charged particles (I), and on the distribution of momentum and charge in the central region of these events (II). A discussion of resonance contributions to the jet containing the trigger particle is given in (20).

The organization of the paper is as follows: In Section 2, a brief review is given of the main features of the apparatus and data reduction, and the parameters used are defined. In

Section 3 we discuss correlations among pairs of particles on the AWAY side (azimuthal angle from the trigger particle $> 90^{\circ}$), presenting evidence for jet-like structures. This extends an analysis initiated in II. In Section 4 we discuss two methods of isolating and analysing jets. In Section 5 we present the results from applying one of these methods to the data. Section 6 contains the summary and conclusions. In two appendices a simple model of jet events is introduced (A), and the two methods of jet analysis are compared on the basis of this model (B).

2. APPARATUS, DATA SAMPLES, AND DEFINITION OF VARIABLES

2.1 Apparatus

The experiment was carried out at the CERN ISR, using the Split Field Magnet (SFM) and its detector (SFMD) in conjunction with the British-Scandinavian Wide Angle Spectrometer (WAS) which was placed at the SFM in a direction perpendicular to the bisector of the acute angle between the two colliding proton beams.

The main components of the apparatus, WAS , SFM , and SFMD are described in paper I and in references given there. A schematic drawing of the set-up is shown in fig. 1.

The WAS was used to detect and analyse the track of a high p_T charged particle, and to give a trigger for registration of the event with the SFMD.

2.2 Data samples

The trigger particle in WAS could be unambiguously identified as $\pi^{\pm}$, $K^{\pm}$, p or $\bar{p}$ in the c.m.s. momentum range 0.5-4.5 GeV/c (see paper I for details). For momenta above 4.5 GeV/c the particle identity could only be classified as "heavy particle" or π.

From the SFMD signals the tracks of about 65% of the charged particles emitted from the pp collisions were found and analysed, giving the charge and momentum vectors at the

collision point (see I). In the Lorentz transformation to the c.m.s. system a π mass was used for all the associated particles, except for positive particles with $|x| > 0.4$, where a proton mass was used (x is the Feynmann variable, $x = 2p_{\ell}^{cms}/\sqrt{s}$).

Table 1 gives the numbers of events, classified according to the momentum of the trigger particle (for a more detailed breakdown of the sample, see II). The data used for the present study were taken at a c.m.s. energy of $\sqrt{s} = 52.6$ GeV.

During the experiment a set of events forming an almost unbiassed sample of inelastic pp collisions was registered for calibration purposes. It was obtained by using the SFMD in a self-triggering mode, requiring at least two track candidates in the detector. In the analysis it was required that at least two tracks could be reconstructed per event. This trigger was sensitive to $\sim 95\%$ of the total inelastic cross-section. The resulting sample (with the elastic events removed) consists of 23,340 events, and is called the Minimum Bias sample.

2.3 Variables

The events are described in a right-handed Cartesian coordinate system, where the x-axis is pointing radially outwards from the ISR centre, the y-axis is the bisector of the acute angle between the beams, and the z-axis is pointing vertically upwards (see fig. 1). The direction of the trigger particle in WAS is close to the direction of the negative x-axis. In the c.m.s. of the collisions the y-axis is along the beams.

$\vec{p} = (p_x, p_y, p_z)$ is the momentum vector of a particle in the c.m.s.

$y = \frac{1}{2} \ln \frac{E + p_y}{E - p_y}$ is the longitudinal rapidity in the c.m.s., where $E = \sqrt{\vec{p}^2 + m^2}$ is calculated with the mass assignment as described above.

$p_T = \sqrt{p_x^2 + p_z^2}$ is the transverse momentum in the c.m.s.

ϕ is the azimuthal angle around the beam direction in the c.m.s. $\phi = 0$ in the direction of the positive x-axis (away from the trigger direction). We define $|\phi| \leq 180^\circ$, and we shall refer to the regions $|\phi| > 90^\circ$ and $|\phi| < 90^\circ$ as the TRIGGER side and the AWAY side, respectively.

p_{TRIG} is the c.m.s. momentum of the trigger particle ($\approx p_T$ of the trigger particle).

q_T , $q_\parallel$ are the transverse and longitudinal momentum components of a particle with respect to an axis different from the collision axis (e.g. a suitably defined jet axis).

2.4 Acceptance

The WAS has a solid angle of $\sim 4 \times 10^{-3}$ sr , with a momentum resolution typically of $\Delta p/p \approx 3\%$ at $p \approx 3$ GeV/c.

In the SFMD the momenta are measured with greatly varying precision owing to the particular form of the magnetic field and the geometry of the detector (see papers I and II).

A requirement of $\Delta p/p < 0.5$ has consequently been made on the relative momentum measurement error. An acceptance table was obtained by comparison of the particle density observed in Minimum Bias events with known inclusive spectra (11-15). In the central region the useful $|\phi|$ range on the AWAY side is essentially restricted to $|\phi| < 30^{\circ}$ (see paper II). Fig. 2 shows the acceptance in this region as a function of $|y|$, in two $|\phi|$ bins and in three bins of p_T, for positive and negative particles, respectively. Since the momentum resolution has not been unfolded the acceptance exceeds one in some regions.

The results presented in the next section, on correlations between pairs of AWAY side particles, have been corrected for acceptance effects by giving weights to the observed particles according to the acceptance table.

For the more complicated jet analysis presented in Section 5 it is not practical to correct for acceptance effects in this way. Instead comparisons to a simple model of jet events (see appendix A) are made, where the SFM acceptance is incorporated in the model predictions.

3. PAIRS OF PARTICLES ON THE AWAY SIDE

In this section we study pairs of particles on the AWAY side, when both particles have transverse momenta p_T larger than a chosen value p_T^o. The trigger momentum was in the range $2.5 < p_{TRIG} < 6.0$ GeV/c. The cuts $|\phi| < 30^{\circ}$ and $\Delta p/p < 0.5$ are required throughout. If more than two particles satisfying these requirements are present, all possible pairs are taken. Each pair has been given a weight equal to the product of the inverse values of the acceptances for the two particles.

Fig. 3 shows the distribution of the rapidity difference $\Delta y = |y_1 - y_2|$, for pairs of AWAY side particles with $p_T > p_T^o$, for $p_T^o = 0.4$, 0.8 and 1.2 GeV/c, for a) neutral pairs and b) doubly charged pairs. A similar plot, uncorrected for acceptance, was shown in paper II, for $p_T^o = 0.8$ GeV/c.

Also shown are distributions obtained by combining each of the particles with particles also satisfying the cuts, but chosen from other events in the same sample. This procedure gives distributions which are uncorrelated in the sense that internal correlations are washed out, but which still maintain correlations to fixed features of the events, such as the collision axis, the trigger direction and, to some extent, the magnitude of p_{TRIG} . They also contain the influences of the applied cuts, and possible residual effects from the acceptance variations.

The "mixed event" distributions have the same shapes as the real distributions for $\Delta y > 1$, but do not show the pronounced peak which is observed in the real data at small Δy . Therefore it is natural to take them as background to a correlation phenomenon, and they have been normalized to the real distributions in the region $\Delta y > 1$.

Additional support for this interpretation comes from a comparison of figs. 3a and b which show that the real data for neutral and doubly charged pairs agree well at large Δy . Since the positive/negative ratio is close to 1 (being $\sim$ 1.20), this is to be expected if the pairs at large Δy are uncorrelated.

The difference between the real and background distributions, which we call the signal, decreases when p_T^o is increased, but increases relative to the background. The signal is stronger for neutral than for doubly charged pairs.

The signal for neutral and doubly charged pairs with $\Delta y < 1$, is shown as a function of p_T^o in fig. 4 . In both cases there is a roughly exponential decrease with p_T^o . One notices that the ratio between the neutral and doubly charged signals stays constant, at a mean value of 1.8 .

The width, $< \Delta y >$, of the signal seen in fig. 3 is shown in fig. 5 as a function of p_T^o . For neutral pairs $< \Delta y >$ is seen to decrease with p_T^o , whereas it is consi-

stent with being constant for doubly charged pairs. This difference in behaviour can be attributed to the production of vector mesons added to a component with an approximately constant $\langle \Delta y \rangle$, as for the doubly charged pairs. This is because the mean rapidity separation of the pions from the decay of ρ^0's at low p_T is around 1, whereas the bias introduced by a p_T cut on both pions decreases this value (see eq. (1) below). A quantitative estimate shows that the observed decrease in $\langle \Delta y \rangle$ can be explained by a ρ^0 content of the order of 10%.

The dashed line on fig. 5 shows the result of a model calculation which will be discussed in Section 5.

Figs. 6a and b show the distributions of invariant mass M, corresponding to figs, 3a and b, with the background mass distribution subtracted. All AWAY side particles have been taken to be pions. A low mass enhancement is seen, which widens with increasing p_T^0.

The connection between M, the transverse momenta p_{T1} and p_{T2}, the azimuthal difference $\Delta\phi$, and Δy is given by:

$$M^2 = 2m^2 + 2\sqrt{p_{T1}^2 + m^2}\sqrt{p_{T2}^2 + m^2}\cosh\Delta y - 2p_{T1}p_{T2}\cos\Delta\phi \qquad (1)$$

where m is the pion mass. Thus the widening of the mass distributions is closely related to the fact that the Δy (and $\Delta\phi$) distributions change only slowly with p_T^0 (see discussion below).

No clear ρ^0 signal is seen in fig. 6a, but the data are consistent with a ρ^0 content of the order of 10% of the total neutral signal. The maximum content possible is about 30%. The corresponding mass distributions at lower values of p_{TRIG} are similar to those presented here.

4. SOME METHODS OF JET ANALYSIS

The results presented above on the correlations between pairs of charged AWAY side particles give evidence for the presence of jets in high p_T hadronic collisions. Nevertheless most of the events studied do not show a clear jet at large angles on the AWAY side. This is not surprising in view of the moderate values of p_{TRIG} in this experiment (see table 1), and the fact that neutral particles are not observed.

In the following we attempt to find a general method of classifying particles as to whether they are more likely to belong to an AWAY side high p_T jet, or to a low p_T "background". One can then study in more detail the distribution and internal properties of such operationally defined jets. It must be borne in mind, however, that some of these properties may be induced by the method of selection itself, and thus will not give new information about "real jets", so that several different approaches may be needed to extract the maximum information from the data. In the present section two such methods of jet analysis are introduced, and a short summary is given of a comparison based on the model of jet events presented in appendix A. In Section 5 the model will also be compared to results from the application of one of these methods to the real high p_T data.

4.1 Principal Axis method

This method was developed as an attempt to bring the sphericity analysis used in e^+e^- annihilation experiments (3), into a form suitable for the analysis of pp collisions with high transverse momenta.

In each event that axis is found which minimizes the quantity:

$$\chi^2 = \sum_{q_T < p_T,\, q_{\parallel} > 0} q_T^2 + \sum_{\text{all other}} p_T^2 \qquad (2)$$

where the sums are over AWAY side particles (satisfying $\Delta p/p < 0.5$) and p_T and q_T are the transverse momenta relative to the beam axis and the axis under consideration, respectively. $q_{\parallel}$ is the longitudinal momentum component along the current axis. Thus each particle enters into one of the sums only, according to the values of p_T and $\vec{q}$.

The axis found in this way is taken to represent the jet axis, and the division of particles into two categories simultaneously provides the distinction between jet particles ($q_T < p_T$, $q_{\parallel} > 0$), and other AWAY side ("background") particles ($q_T > p_T$ or $q_{\parallel} < 0$).

4.2 Gaussian Smearing method

As a jet is in general expected to be a cluster of particles with large total p_T, a method was devised in which the density of transverse momentum in the (y , ϕ) plane on the AWAY side is represented by a smooth, two-dimensional function $G(y , \phi)$, so that it is possible to look for a large, localized transverse momentum in this plane.

The method was applied in the following way: In an event with N particles on the AWAY side (satisfying the requirement $\Delta p/p < 0.5$), N two-dimensional Gaussians in y and ϕ are formed, centred at the position of each particle, with fixed widths S_y , S_ϕ and heights proportional to the p_T of the particles. The N Gaussians are summed to form the function $G(y , \phi)$:

$$G(y,\phi) = \sum_{i=1}^{N} p_{Ti} \exp\left(-\frac{(y-y_i)^2}{2S_y^2} - \frac{(\phi-\phi_i)^2}{2S_\phi^2}\right) \qquad (3)$$

A jet is identified by a maximum of this function above a certain threshold. All particles inside the contour at half maximum of $G(y , \phi)$ are included in the jet. An example of an event analysed in this way is shown in fig. 7.

The position of the maximum defines the rapidity, y_J , and azimuth, ϕ_J , of the jet. Its transverse momentum, p_T^J , is defined as the height of the peak. The resulting values of y_J , ϕ_J and p_T^J are found to be close to those obtained from the vector sum of the particles' momenta.

4.3 Comparison of methods on Monte Carlo jets

A detailed comparison of the ability of these methods to reconstruct Monte Carlo generated jets superimposed on Minimum Bias (background) events (see app. A) is given in appendix B.

This comparison shows that a necessary condition for the methods to give sensible results is that the observed jet transverse momentum, p_T^J , should be larger than 1.5 GeV/c. When this is fulfilled there are no major differences between the methods, but the Gaussian Smearing method is found to be somewhat better in representing the input jet when the smearing widths, S_y and S_ϕ , are suitably chosen. The best values are found to be $(S_y , S_\phi) = (0.5 , 30^o)$.

As the sample of jets found depends on the transverse widths S_y and S_ϕ used, the resulting distributions of transverse variables (e.g. $\Delta y = |y_J - y|$ or q_T) depend strongly on the choice of these widths. The longitudinal structure of the observed jets and their distribution in angle and momentum are however relatively independent of such details.

5. HIGH P_T JETS FOUND BY THE GAUSSIAN SMEARING METHOD

Following the conclusion of the last Section, we shall now present results from an analysis based on an application of the Gaussian Smearing method to the AWAY side particles in the high p_T triggered events and to the Minimum Bias events. The parameters (S_y , S_ϕ) are kept fixed at the values $(0.5 , 30^o)$ and the observed jet transverse momentum, p_T^J , is required to be larger than 1.5 GeV/c. Unless otherwise stated the rapidity and azimuth of the jet axis are

restricted to $|y_J| < 2$, $|\phi_J| < 30^o$ in order to be in a region where the jet acceptance (see appendix B) is reasonably high.

Application of the method gives for each found jet a set of measured quantities characterizing the jet. These include the parameters y_J , ϕ_J and p_T^J (see Section 4.2) for the jet as a whole, and quantities that can be formed on the basis of the charges, Q_i , and momentum vectors, $\vec{p}_i$, of the observed charged particles classified as jet particles.

The distributions of such quantities are studied in samples of high p_T triggered events for specified ranges of the trigger momentum and in the Minimum Bias sample.

The observed distributions obviously deviate from the ideal distributions for the whole physical jet due to the lacking detection of neutral particles and the imperfect detection of charged particles, and due to the effects of the analysis method and experimental cuts. We attempt to overcome these limitations by using the model of high p_T jet events presented in appendix A as a tool to determine corrected distributions in y_J , ϕ_J and p_T^J , as well as the particle multiplicity and momentum structure of the jets.

In the model, a high p_T jet event is represented by a jet superimposed on a "background" consisting of a randomly chosen Minimum Bias event (with diffractive events suppressed). The rapidity, azimuth, transverse momentum and multiplicity of the jet are chosen from specified distributions. The distributions characterizing the internal structure of the jet are fixed, as specified in appendix A. The jet particles are subjected to a simulated detection with the SFMD and the resulting events have been analysed with the Gaussian Smearing method in the same way as the real data.

The corrected distributions of y_J , ϕ_J etc. are determined as those that must be given to the model jets in order

to reproduce the distributions obtained from real data as closely as possible.

In principle it is quite difficult to correct the observed distributions, even if the model used describes the internal structure of the jets well. This is because the corrections to the y_J , ϕ_J , p_T^J and multiplicity distributions are a priori coupled and the problem therefore multidimensional.

We find however that it is possible to correct independently the y_J and ϕ_J distributions, as well as the mean multiplicity in the jets at the various values of p_{TRIG} . Using the parameters of these corrected distributions in the model, we have then determined corrected distributions of p_T^J .

We find that the jet model with the set of parameters determined this way describes all of our data consistently.

The results of this analysis necessarily depend, at least to some degree, on the model we have employed. We therefore show the observed distributions, uncorrected for acceptance, as well as the model predictions for these distributions, using the full set of corrected distributions. It is then possible to check other models against our data using our acceptance (fig. 2), and analysis method on model events.

5.1 Frequency of high p_T jets

The fraction of high p_T triggered events which contain an AWAY side jet as defined by the method is shown in fig. 8 as a function of p_{TRIG} . The fraction increases from values around 0.03 at the lowest values of p_{TRIG} to values around 0.40 at $p_{TRIG} \approx 5$ GeV/c.

The point at $p_{TRIG} = 0$ shows the frequency of jets observed in Minimum Bias events in the same part of the apparatus.

Also shown on the figure are lines corresponding to the number of jet events per trigger found in Monte Carlo events, which have one jet per event with the x component of the jet

momentum $p_{xJ}^{MC} = p_{TRIG}$ (dashed line, see fig. B3), and $p_{xJ}^{MC} = p_{TRIG} - 0.8$ GeV/c (dashed-dotted line). The value 0.8 GeV/c is an estimate of the average recoil of the background event based on data given in paper I and II.

The comparison of the data with the model curves shows that although we only find 0.2-0.3 jets per event at $p_{TRIG} = 3$-4 GeV/c, this frequency is consistent with the presence of about one AWAY side jet per triggered event, provided that a recoil of roughly 0.8 GeV/c taken up by the background event is taken into account. We shall return to this question in more detail in the discussion of the p_T spectrum of jets below.

5.2 Distribution of jets in y_J, ϕ_J and p_T^J -

The observed distributions in rapidity, y_J and azimuth ϕ_J, of the jet axes are shown in figs. 9 and 10 for the AWAY side jets in the high p_T triggered events in four intervals of p_{TRIG}, and for jets observed in the same region of the apparatus in Minimum Bias events. For the ϕ_J distribution the jet rapidity is restricted to the interval $|y_J| < 1$.

From the relative changes of the distributions with increasing p_{TRIG}, it is directly seen that the increase in the number of observed jets per event is strongest at small y_J and ϕ_J. Both distributions thus become narrower with increasing p_{TRIG}.

Although irregularities due to the acceptance are clearly present in the observed distributions, the general shapes are similar to Gaussians.

The corrected distributions in y_J and - for the high p_T events - ϕ_J are consequently assumed to be Gaussians, and are characterized by widths, σ_y^J and σ_ϕ^J, obtained as described above.

The observed and corrected widths, σ_y^J and σ_ϕ^J, are shown in fig. 11 as functions of p_{TRIG}. The points at

$p_{TRIG} = 0$ represent Minimum Bias events. The errors given are only statistical.

The variations of the corrected widths with p_{TRIG} are consistent with being linear over the range considered. The slopes from linear fits are $d\sigma_y^J / d\, p_{TRIG} = -0.27 \pm 0.06$ $(GeV/c)^{-1}$ and $d\sigma_\phi^J / d\, p_{TRIG} = -4.3^o \pm 0.6^o$ $(GeV/c)^{-1}$. The latter value should however be regarded with some caution, as the accessible range of ϕ_J is limited to $|\phi_J| < 30^o$, and the corrected values of σ_ϕ^J are of a similar magnitude at small values of p_{TRIG}.

The quality of the representations thus obtained for the distributions of y_J and ϕ_J may be judged from a comparison of the data points in figs. 9 and 10 with the histogram lines. These represent the results of a model calculation using the final set of parameters. For the ϕ_J distribution in Minimum Bias events, the input distribution was flat.

If AWAY side jets and single AWAY side particles with high transverse momentum originate from the same sources, one would expect that they have similar rapidity distributions. This seems indeed to be the case, as shown by the comparison in fig. 11 of the corrected σ_y^J's with the similar widths of the (acceptance corrected) rapidity distributions of single AWAY side particles with $p_T > 0.8$ GeV/c.

(Statistical limitations to our determination of the acceptance preclude a comparison with the distribution of single particles of higher p_T).

In order to investigate the distribution of the transverse momentum of jets recoiling from a trigger particle with a given momentum, we show in fig. 12 the quantity

$$\frac{1}{N_{TRIG}} \cdot \frac{1}{p_T^J} \frac{dn}{dp_T^J}$$

as a function of the observed p_T^J in four intervals of p_{TRIG} and for Minimum Bias events. Here the rapidity of the jet axis has been restricted to the region $|y_J| < 1$.

The observed distributions are consistent with being exponential for p_T^J between 1.5 GeV/c and ~ 5 GeV/c.

As demonstrated by fig. 8 above, it is possible to account for the observed frequency of AWAY side jets by specifying in the model, which has one jet per event, suitable fixed values of p_{xJ}^{MC} as a function of p_{TRIG}.

The resulting prediction for distribution of the observed p_T^J is however not in agreement with the data. This is demonstrated in fig. 12 by the dashed line, which shows the model prediction obtained with a fixed $p_{xJ}^{MC} = 2.7$ GeV/c. This value corresponds to the interval $3.5 < p_{TRIG} < 4.5$ GeV/c, but the predicted distribution is clearly different from the distribution of the data points for the same range of p_{TRIG}.

In a simplified picture of high p_T proton-proton collisions the trigger particle and the AWAY side jet originate from scattered constituents of the protons, and one might assume that the background recoils from the trigger particle with a definite momentum. It is therefore natural to take a δ-function at a fixed value of p_{xJ} as a first approximation to the distribution of p_{xJ} at a given value of p_{TRIG}.

A more realistic picture must however include some smearing of the distribution of the jet transverse momentum due to several contributions. Firstly the trigger particle takes a fraction of the momentum of the TRIGGER side jet which varies from event to event. Secondly the transverse motion of the constituents, which is responsible for at least some of the lack of balance of transverse momentum between the two jets, has a distribution with a certain width.

We therefore attempt to describe the distributions of p_T^J in the various intervals of p_{TRIG} by input distributions to the model of the form:

$$\frac{1}{p_T^{JMC}} \frac{dn}{d p_T^{JMC}} \propto \begin{cases} \exp(-a p_T^{JMC}) & \text{for } p_T > p_T^o \\ 0 & \text{for } p_T \leq p_T^o \end{cases} \qquad (4)$$

suggested by the distributions of the observed p_T^J . The normalization is determined by the parameter p_T^o such that the frequency of "observed" jets in model events is the same as the frequency of observed jets in real events (fig. 8).

When the Monte Carlo jets in our model are generated with p_T^{JMC} distributions according to (4) we also find exponential distributions of the output, i.e. the jets found when the model events are analysed. We therefore determine the corrected p_T^J distributions as the distributions of this form which must be given to the model jets to reproduce as closely as possible the observed distributions. Here we make use of the already determined y_J and ϕ_J distributions, as well as the corrected jet multiplicities discussed below.

Fig. 13 summarizes the observed and corrected values of the slope, a , as a function of p_{TRIG} . As above, the points at $p_{TRIG} = 0$ represent the Minimum Bias events.

Since the Gaussian Smearing method cannot be used to find jets with transverse momenta below 1.5 GeV/c, the normalization poses a special problem. In equation (4) this is expressed through the parameter p_T^o , but as this involves an extrapolation below 1.5 GeV/c (see fig. 14), it is clear that other representations are possible.

The mean transverse momentum, $\langle p_T^J \rangle$, of the jets can be calculated from the values of p_T^o and the slopes, a . p_T^o and $\langle p_T^J \rangle$ are shown as functions of p_{TRIG} in fig. 14. The values of $\langle p_T^J \rangle$ are in good agreement with the values of $p_{\chi J}^{MC}$ obtained from fig. 8 as discussed above.

The corresponding average recoil of the background event increases slowly with p_{TRIG}, and reaches values around 1.0 GeV/c at the highest values of p_{TRIG}.

The lines in fig. 12 show the model predictions corresponding to the data points using the full set of corrected parameters for the distributions and multiplicities of the jets.

In the case of the Minimum Bias events, the normalization of the corrected y_J, ϕ_J and p_T^J distributions determines the inclusive rate of jets with a total transverse momentum $p_T > 1.5$ GeV/c to be 0.30 ± 0.05 jets/event. The mean transverse momentum of these jets is 1.9 GeV/c.

From the normalization and the parameters determined above, we can write an approximate formula for the inclusive jet cross section in the range $1.5 < p_T \lesssim 3$ GeV/c:

$$\frac{1}{\sigma_{inel}} \frac{d\sigma}{dy\, dp_T} = 10\, p_T e^{-3.1 p_T} e^{-y^2/8.8} \qquad (5)$$

This formula neglects the dependence of σ_y on p_T, but is estimated to represent the cross section with an uncertainty of less than a factor 1.5 in the indicated range of p_T.

As an a posteriori check, we have used the formula together with the fragmentation function given in appendix A (equation (A3)) to "predict" the inclusive π^0 spectrum at 90^0 in the c.m.s. . The result agrees within 20% with the measured spectrum in the p_T interval 1.5-2.5 GeV/c, but falls below at higher p_T due to the exponential form used in (5).

Our estimate of the ratio of inclusive jet production to inclusive π^0 production at the same p_T at 90^0 in the c.m.s. is then 8 ± 3 at $p_T = 1.5$ GeV/c and 16 ± 5 at $p_T = 2.6$ GeV/c (corresponding to $x_T = 2p_T/\sqrt{s} = 0.1$).

The corresponding ratio at a fixed energy, E, can be very different as the jet masses are quite large, being around 2 GeV/c^2. If the p_T spectrum given by equation (5) is used above a lower limit p_T^o = 1 GeV/c, and all the jet particles are assumed to be pions, we find the value 150 for the ratio at E = 2.6 GeV.

Feynman, Field and Fox (29) have predicted the ratio of inclusive quark production to inclusive π^o production at 90° in the c.m.s. on the basis of considerations motivated by QCD. At $\sqrt{s}$ = 53 GeV, and x_T = 0.1 the predicted value is $\sim$ 200.

One may argue that the energy of a jet is likely to be close to the energy of a scattered parent quark, whereas its momentum is likely to be quite different from the momentum of the quark due to the large difference in mass between the jet system and the parent quark.

If, on the basis of such arguments, one compares the theoretical prediction with our measured ratio at fixed E, the agreement is good.

It is clear however that the large difference between the jet to π^o ratio at fixed p_T and at fixed energy in the range studied here means that a sharp comparison with the theoretical prediction of the quark to π^o ratio (where $E \approx p_T$) can only be made at higher values of p_T.

A fraction of 0.10 of the jet events in the Minimum Bias sample with $p_x^J < 0$ also have an observed jet with $p_T^J > 1.5$ GeV/c on the AWAY side. This is very close to the fraction of events with a single particle trigger with p_{TRIG} = 1.9 GeV/c that have an observed AWAY side jet (see fig. 8). This is what one would expect if the jet fragmentation on the two sides occurs independently, given that a single high p_T trigger on the average takes almost all the momentum of the jet it belongs to.

5.3 Mean multiplicity and momentum distributions in the jets

The mean observed multiplicity of charged particles, $\langle n_{ch}^{J} \rangle$, of the jets is shown in fig. 15 as a function of p_{TRIG}.

From the analysis of model events we find that there is a linear relationship between the "observed" charged multiplicity and $\langle n_{ch}^{MC} \rangle$, which does not depend significantly on the value of p_{xJ}^{MC} between 2 and 4 GeV/c. In our model $\langle n_{ch}^{MC} \rangle$ is 60% of the total multiplicity, $\langle n \rangle$, which is an input parameter.

We have used the linear relationship to correct the observed multiplicities presented above. The results are shown in fig. 15. The errors shown are statistical only.

We have checked that the uncorrected values of $\langle n_{ch}^{J} \rangle$ are reproduced by the model using the complete set of model parameters.

We have also found that the observed dispersion of the charged particle multiplicity, $\sigma(n_J^{ch})$, is reproduced quite well by the model as a function of p_{TRIG}. This indicates that the multiplicity distribution in the jets is nearly a Poisson distribution at the values of p_{TRIG} investigated.

In order to compare the multiplicities with those observed in e^+e^- annihilations and νp scattering, we want to estimate the c.m.s. energy, $\sqrt{\hat{s}}$, of the system consisting of the TRIGGER side jet and the AWAY side jet. In our model we approximate this by the c.m.s. energy of the trigger particle and the AWAY side jet. We find that

$$\sqrt{\hat{s}} \approx \sqrt{M_J^2 + 2\, p_{TRIG}(E_J + p_{xJ})}$$

$$\approx 3.0 + 1.4\, p_{TRIG} \quad \text{for } p_{TRIG} \gtrsim 2\ \text{GeV/c} \qquad (6)$$

where M_J is the mass of the jet and E_J is its energy, when $\sqrt{\hat{s}}$ is averaged over jets with the corrected y_J, ϕ_J

and p_T^J distributions. Estimates indicate that the uncertainty in $\sqrt{\hat{s}}$ is less than 0.7 GeV at $p_{TRIG} \gtrsim 2$ GeV/c.

In fig. 15 we have therefore compared our data with half the total charged multiplicity in e^+e^- annihilations (16, 17) observed at a total c.m.s. collision energy of $\sqrt{\hat{s}}$. The uncertainty in our knowledge of $\sqrt{\hat{s}}$ is indicated by horizontal error bars of $\pm$ 0.7 GeV.

From the comparison it appears that the corrected charged jet multiplicity in our case is larger by about 20% than the charged multiplicity in e^+e^- jets.

The most important systematic uncertainty in the corrected multiplicities comes from the assumption made in the model about the distribution of the fractional longitudinal momentum, z, which is taken to be exponential all the way to zero. 40 per cent of the corrected multiplicity comes from the region $z < 0.1$, where our acceptance is low, and the z-distribution consequently least well determined.

From the corrected charged multiplicity given in fig. 15, one can calculate the multiplicity above a given z^o from:

$$\langle n_{ch}^J(z^o) \rangle = \langle n_{ch}^J \rangle \frac{e^{-\langle n \rangle z^o} - e^{-\langle n \rangle}}{1 - e^{-\langle n \rangle}} \qquad (7)$$

where $\langle n \rangle = \langle n_{ch}^J \rangle / 0.6$ is the total multiplicity. For $z^o = 0.2$ we find $\langle n_{ch}^J (0.2) \rangle = 1.10 \pm 0.03$, independent of p_{TRIG} over the range studied. This is in good agreement with data for u-quark fragmentation from νp scattering (18), where the number of charged particles with $z > 0.2$ is found to be $1.07 \pm .08$ in a similar range of jet energies.

For the directly observed particles in a jet we define a fractional longitudinal momentum, ζ, on the basis of the <u>observed</u> jet momentum, p_J, as:

$$\zeta = \vec{p} \cdot \vec{p}_J / |\vec{p}_J|^2 \qquad (8)$$

With this definition the values of ζ always sum up to 1 for the observed jet particles.

The distribution of ζ is shown in fig. 16 for four intervals of p_{TRIG}. The distributions are approximately exponential, except for the spike at $\zeta = 1$ due to one particle jets, and a strong depletion near $\zeta = 0$ (reflected near $\zeta = 1$), caused by the loss of very low momentum particles. The points at $\zeta = 1$ have been calculated as the frequency of one particle jets multiplied by the inverse bin-width, in analogy to the other points.

The histogram line on the figure shows the ζ-distribution obtained from model events with parameters corresponding to $p_{TRIG} = 2.9$ GeV/c. The agreement with the data points for $2.5 < p_{TRIG} < 3.5$ GeV/c is good, and the agreement between the model calculations and the data at the other values of p_{TRIG} is equally good.

The distributions are seen to scale approximately with p_{TRIG} in the range $0.2 < \zeta < 0.8$, although a slight variation of the slope can be recognized. We have made exponential fits to the ζ-distributions in the range 0.2-0.8. The resulting slope, b, is shown as a function of p_{TRIG} in fig. 17.

From the model calculations used to correct the charged multiplicities above, it was also possible to relate the slopes similarly defined for the reconstructed Monte Carlo jets to the slopes of the input z-distributions. In this way we have obtained corrected slopes, which are also shown in fig. 17.

Consistency of the corrections requires that these slopes are equal to the total corrected mean multiplicity $\langle n \rangle = \langle n_{ch}^{J} \rangle / 0.60$ obtained from fig. 15. This is indeed seen to be the case.

From the published distributions of

$$x_{\parallel} = \frac{\vec{p} \cdot \vec{p}_J}{|\vec{p}_J|} \cdot \frac{2}{\sqrt{s}} \qquad (9)$$

in e^+e^- annihilations (17) and the similarly defined quantity in charged current νp reactions (18), we have obtained exponential slopes in the interval $0.2 < x_{\parallel} < 0.8$ which are also shown on the figure. For the e^+e^- jets the distributions were obtained from jets recoiling from another jet, which included a particle with $|x_{\parallel}| > 0.3$. In the case of νp collisions, we have taken the sum of the u-quark fragmentation functions $D_u^+(x_{\parallel})$ and $D_u^-(x_{\parallel})$ given by the authors.

The variable $x_{\parallel}$ used in these distributions is normalized to the jet energy, E_J , whereas the z variable is normalized to the (total) jet momentum. We have tried to estimate the effect of this difference by studying the distributions in the model events. From exponential fits in the interval $0.2 < x_{\parallel} < 0.8$ we find that the slopes of these distributions (see fig. 17) are approximately 15% larger than the corresponding slopes of the z-distributions.

The slopes of the $x_{\parallel}$ -distributions from the different sources show a strikingly good agreement. This indicates that the structure of the jets is very similar in the high $x_{\parallel}$ region, $x_{\parallel} > 0.2$.

A direct comparison of the $x_{\parallel}$ -distribution from our model events and from the e^+e^- jets is shown in fig. 18. We have here taken model parameters corresponding to $p_{TRIG} =$ 1.9 and 2.9 GeV/c, and compared to e^+e^- data for which the total c.m.s. energy is close to the estimated values of $\sqrt{\hat{s}}$ at these values of p_{TRIG} .

There is a good general agreement between the distributions, except for a small (10-20%) overall difference in normalization, and an excess of particles at very low $x_{\parallel}$ in the high p_T jets. Although this is the region where the distribution is least constrained by the data, the comparison in fig. 16 between the data and model prediction at small ζ shows that it is not possible to accomodate the change in the $x_{\parallel}$ -distribution which would be necessary

in order to bring it into agreement with the corresponding distribution from e^+e^- jets.

We therefore conclude that the difference in multiplicity (see fig. 15) between the high p_T jets from proton-proton collisions and the e^+e^- jets is at least partly due to a difference in structure at small $x_{||}$.

According to current understanding of the basic processes involved in the different reactions there is no a priori reason why jets from different types of reactions should have exactly the same structure. In e^+e^- annihilations several quark types contribute to the jets (u,d,s,c), in charged current νp reactions only u-quarks contribute, and in high p_T proton-proton collisions more than half of the AWAY side jets may originate from gluons (19).

In paper II we studied the distribution of the x_E variable, defined as the fraction of p_{TRIG} balanced by a given AWAY side particle. We found that the distribution of x_E is approximately exponential with a slope around 8 , and that it scales for $p_{TRIG} \gtrsim 3$ GeV/c and $x_E > 0.3$. Modifications to take into account the momentum accompanying the trigger particle increased the slope to about 9 . We have checked that the x_E distribution is well reproduced by the model of jet events with the final set of parameters. The reason for the difference in slope between the x_E - and z-distributions is mainly the incomplete balance of the trigger momentum by the AWAY side jet.

Some information on the transverse structure of the jets can be obtained from the observed width, $\langle \Delta y \rangle$, of the correlated pairs of AWAY side particles with a fixed p_T cut, p_T^o , discussed in Section 3.

If the average internal transverse momentum, $\langle q_T \rangle$, in the jets is parametrized (see appendix A) as

$$\langle q_T \rangle = q_0 + 0.8\, z\,(1 - z) \quad [\text{GeV/c}] \qquad (10)$$

q_o can be determined from a comparison of the $<\Delta y>$ obtained from the analysis of model events using various values of q_o with the $<\Delta y>$ obtained from our data (see fig. 5). Comparing for doubly charged pairs (in order to avoid effects due to vector mesons) with $p_T^o = 1$ GeV/c , we find that $q_o = 0.34 \pm 0.08$ GeV/c , in good agreement with the value 0.3 GeV/c used in the model calculations above. The variation of $<\Delta y>$ for doubly charged pairs with p_T^o in fig. 5 is reproduced by the model.

The z-dependence of $<q_T>$ cannot be determined by this method. If $<q_T>$ is assumed to be independent of z , the variation of $<\Delta y>$ with p_T^o is also reproduced, and the value of $<q_T>$ is found to be 0.50 ± 0.08 GeV/c.

5.4 Charge of the jets

The observed average charges, $<Q_J>$, of the jets found by the Gaussian Smearing method are shown in fig. 19 for the six different types of trigger particles.

From fig. 2 it can be seen that the acceptance for positive and negative particles is not very different for reasonably high p_T , whereas for very low p_T large differences occur. We have therefore imposed a cut $p_T > 0.3$ GeV/c on the particles used in forming Q_J . Furthermore we have checked that increasing this cut to 0.5 GeV/c does not change the results very much.

Fig. 19 shows a clear correlation in the direction of charge compensation between the charge of the trigger particle and the charge of the AWAY side jet for $\pi^\pm$ and $K^\pm$ triggers. Opposite to p triggers $<Q_J>$ is consistent with the values found with π^+ and K^+ triggers, whereas the situation for $\bar{p}$ triggers is inconclusive.

It is not possible to correct the values of $<Q_J>$ for the effects of acceptance and selection criteria without introducing a more complicated jet model. This is because the z-distributions for positive and negative particles could in

principle be different, as they are in fact observed to be in charged current νp reactions (18).

By varying the proportions of positive and negative particles in the model jets without altering the z-distribution, and thereby $\langle n \rangle$, we find that the observed values of $\langle Q_J \rangle$ opposite to π^- and π^+ triggers are reproduced for input total jet charges of $+0.06 \langle n \rangle \approx 0.30$ and 0.00 respectively. $\langle n \rangle$ is the mean total multiplicity of the jets which is close to 5.

We have investigated the dependence of $\langle Q_J \rangle$ on p_{TRIG}, and found no significant variation.

The average charge per (observed) jet particle is shown in fig. 20 as a function of ζ for positive and negative triggers and in two intervals of p_{TRIG}. The distributions are rather flat, although with a possible weak tendency for the charge per particle to increase with ζ, especially for the large trigger momenta. The partial compensation of the trigger charge by the jet is seen to extend rather uniformly over ζ. A possible exception is the region of large ζ for $p_{TRIG} < 1.5$ GeV/c, i.e. the region where the momentum of the jet particle is often comparable to, or larger than p_{TRIG}. Here the charge per particle seems to be equal in magnitude for positive and negative triggers, but the statistics prevents us from drawing any strong conclusions on this point.

In the jet model with total jet charge $\langle Q_J \rangle = 0.06 \langle n \rangle$ and 0.00, the charge per charged jet particle are 0.10 and 0.00, respectively. The model would therefore predict a constant difference of 0.10 between the charge per particle opposite to positive and negative triggers. This is consistent with the data.

The observation of a correlation between the charge of the trigger particle and the charge carried by the AWAY side jet indicates an exchange of charge between the two scattering systems. In a hard collision model involving quarks and gluons,

this could happen either during the hard collision, e.g. by interchange of a quark, or during the subsequent soft rearrangement of quantum numbers. The fact that the correlation extends over the whole jet makes the first possibility the more likely.

There are also strong charge correlations present within the jet. This is demonstrated in fig. 21, where the average charge per (observed) jet particle is shown as a function of z, with the requirement that z of the fastest observed particle in the jet, z_{max}, is restricted to the intervals $0.4 < z_{max} < 0.6$ and $0.6 < z_{max} < 0.8$, and that it is of a definite charge. Furthermore particles with $p_T < 0.3$ GeV/c have been excluded from the plot.

In both intervals of z_{max}, there is a compensation of the leading charge by other jet particles.

For positive jet leaders, and possibly for negative jet leaders with $0.4 < z_{max} < 0.6$, the charge per particle for other particles in the jet is consistent with being independent of z, whereas for negative jet leaders with $0.6 < z_{max} < 0.8$ it shows a strong rise with z.

6. SUMMARY AND CONCLUSIONS

In the course of a study of proton-proton collisions at a c.m.s. energy $\sqrt{s} = 52.6$ GeV, in which an identified, charged hadron with large transverse momentum is emitted near 90° in the c.m.s., we have investigated jet-like structures among the other charged particles in the events.

A study of AWAY side particles with transverse momenta p_T p_T°, where p_T° is varied, shows that there is a narrow spike at small values of the rapidity difference, Δy. The signal, obtained by subtracting a randomized background normalized in the region $\Delta y > 1$, decreases exponentially with p_T° in the range $0.2 < p_T^\circ < 1.4$ GeV/c. The signal for pairs of particles with opposite charge is a factor 1.8 larger than the signal for doubly charged pairs.

The width, $\langle \Delta y \rangle$, of the signal from doubly charged pairs, is consistent with being independent of p_T^o. The signal from neutral pairs shows a decrease of $\langle \Delta y \rangle$ which could be accounted for by ρ^o production. These observations are taken as evidence for the presence of jet-like structures among the charged AWAY side particles in the high p_T events.

Two methods for isolating jet-like groups of particles are compared on the basis of a simple model of jet events, in which Monte Carlo generated jets similar to those observed in e^+e^- annihilations are superimposed on Minimum Bias events.

Using one of these methods, results are presented concerning the distribution and internal properties of phenomenologically defined jets.

The data are found to be consistent with having about one AWAY side jet per event for trigger momenta above 2 GeV/c.

A set of parameters is determined for the jet model which consistently describes all of our data on the distribution and momentum structure of the jets. The distributions in y_J and ϕ_J of the jet axes are well represented by Gaussians, with widths that are found to decrease with increasing p_{TRIG}. Thus the jets become more central, and more coplanar with the beam and the trigger particle when the trigger momentum is increased. The p_T^J distribution of the jets is approximately exponential in the range studied, and widens with increasing p_{TRIG}.

The frequency of jets found in Minimum Bias events corresponds to an inclusive rate of 0.30 ± 0.05 jets/event with $p_T > 1.5$ GeV/c.

The corresponding ratio of inclusive jet production to inclusive π^o production at 90^o in the c.m.s. is 16 ± 5 at a fixed $p_T = 2.6$ GeV/c. The corresponding ratio at a fixed energy could be much larger.

The charged multiplicity of the jets is estimated to be $\sim$ 20% higher than the charged multiplicity in e^+e^- jets at c.m.s. energies similar to the estimated c.m.s. energy, $\sqrt{s}$, of the system consisting of the trigger particle plus the AWAY side jet. The charged multiplicity of particles with fractional longitudinal momentum $z > 0.2$ is however consistent with the corresponding multiplicity in u-quark fragmentation observed in νp collisions.

The distribution of fractional longitudinal momentum, z , with respect to the observed jet momentum shows approximate scaling for all values of p_{TRIG} .

The exponential slopes of the $x_{\parallel}$ -distributions, where $x_{\parallel}$ is defined as the longitudinal momentum of a jet particle scaled by the jet energy, are very similar in the range 0.2-0.8 for jets from high p_T proton-proton collisions, e^+e^- collisions and νp collisions. There is an indication that the $x_{\parallel}$ -distribution in high p_T jets is slightly more peaked at small values of $x_{\parallel}$ than in e^+e^- jets.

The charge of the jets partly compensates the charge of the trigger particle, and this charge compensation extends over the whole jet at large values of p_{TRIG} . Inside a jet a charge compensating correlation is seen between the jet leader and other jet particles.

Acknowledgements

During the analysis of the experiment we have enjoyed many stimulating conversations with M. Jacob and P.V. Landshoff.

It is a pleasure to thank the SFM detector group and the staff of the ISR division at CERN for their help, and members of the CERN programming staff for their assistance in the on-line and off-line analysis. We would also like to thank Ph. Dam, B. Guillerminet, P. Herbaleb, J.E. Hooper, D. Korder, E. Lohse, B.N. Mortensen, D.B. Smith and M.-I. Sundell for their contributions and assistance. Some authors (S.A., X. de B.,

H.B.J., A.K., B.L., H.E.M., R.M., and P.V.) acknowledge financial support from CERN during part of the experiment.

We gratefully acknowledge support from the CERN and Rutherford computing facilities and from the computer centres at Bergen, Copenhagen and Lund universities. We also acknowledge loan of electronics from the Laboratory for Nuclear Science of M.I.T.

The experiment was supported by the United Kingdom Science Research Council, The Danish and Swedish Natural Science Research Councils, the Norwegian Research Council for Science and the Humanities, and L'Institut National de Physique Nucleaire et de Physique des Particules, France.

Appendix A. THE JET MODEL

A simple model of the structure of high p_T jet events was developed to serve as a basis for the comparison of jet analysis methods (see appendix B), and for comparison with data (see Section 5), taking into account the effects of SFM acceptance and the selection criteria used in the analysis.

In the model, a high p_T event was represented by a "background" event plus a jet, in the following way:

The background event was a randomly selected Minimum Bias event, with the requirement of a charged particle in the central region ($|y| < 1$), in order to suppress diffractive events.

The jet was generated, using a Monte Carlo method, with distributions in momentum and angle which could be specified freely, and with a particle distribution chosen to simulate jets observed in e^+e^- annihilations (3,16,17) which have momenta similar to those studied here (21).

For most applications the x-component of the jet momentum, p_{xJ}^{MC}, was kept fixed, and the jet rapidity and azimuth, y_J^{MC} and ϕ_J^{MC}, were given flat distributions, or Gaussian distributions with widths σ_y^{MC} and σ_ϕ^{MC}. The jets could also be generated with an exponential p_T distribution:

$$\frac{1}{p_T^{JMC}} \frac{dn}{dp_T^{JMC}} \propto \exp\left(-a p_T^{JMC}\right) \qquad \text{(A1)}$$

The number of particles within the jet was taken to follow a Poisson distribution with a mean multiplicity $\langle n \rangle$, with 33% positive, 27% negative and 40% neutral particles. The momentum components along the jet-axis were distributed according to:

$$\left(\frac{dn}{dz}\right)_n = n(n-1)(1-z)^{n-2} \qquad \text{(A2)}$$

for each fixed multiplicity n, leading to

$$\frac{dn}{dz} = \langle n \rangle^2 e^{-\langle n \rangle z} + \langle n \rangle e^{-\langle n \rangle} \delta(1-z) \qquad \text{(A3)}$$

where z is the fraction of the longitudinal jet momentum taken by the particle. The internal transverse momenta, q_T, in the jet were generated according to:

$$\frac{1}{q_T}\frac{dn}{dq_T} \propto e^{-Bq_T} \tag{A4}$$

with

$$\langle q_T \rangle = \frac{2}{B} = 0.3 + 0.8\,z(1-z) \tag{A5}$$

in order to simulate a "seagull effect".

The SFM acceptance was imposed on the charged particles of the jet by means of an acceptance table (see fig. 2), and all neutral particles were "lost".

Appendix B. COMPARISON OF METHODS OF JET ANALYSIS ON MONTE CARLO JETS

In this appendix we shall compare the two methods of jet analysis, the Principal Axis (PA) method and the Gaussian Smearing (GS) method, introduced in Section 4. The Gaussian Smearing method will be used with two sets of values of the parameters (S_y , S_ϕ), namely GS 1: (0.5 , 30°) and GS 2: (0.75 , 45°). The methods are compared on the basis of the model of jet events described in appendix A.

For the Gaussian Smearing method, results are only shown for $p_T^J > 1$ GeV/c as the method breaks down unless a p_T cut of approximately this value is applied.

Fig. B1 shows, as a function of p_T^J of the found jet, the number of found jets per event, and the mean deviations, $\langle |y_J - y_J^{MC}| \rangle$ and $\langle |\phi_J - \phi_J^{MC}| \rangle$, between the generated and found axis, for the three cases.

The input jets were generated with a fixed $p_{xJ}^{MC} = 3$ GeV/c, and with flat distributions in y_J and ϕ_J inside the intervals $|y_J^{MC}| < 3$, $|\phi_J^{MC}| < 30°$. The mean total multiplicity of the jets was 5 .

One notices that for $p_T^J \lesssim 1.5$ GeV/c the results represent the original jet axis badly in all three cases in the sense that $\langle |y_J - y_J^{MC}| \rangle \gtrsim 0.5$, $\langle |\phi_J - \phi_J^{MC}| \rangle \gtrsim 20^o$. For larger p_T^J the methods all work reasonably well.

Another comparison of the ability of the methods to represent the original jet is made in fig. B2 , which again uses the same input jets, with a mean multiplicity of 5 . The figure shows the number of charged particles found, classified in the four categories:

Jj : identified as jet particle - generated as jet particle
Jb : " " jet " - " " backgr. "
Bj : " " backgr. " - " " jet "
Bb : " " backgr. " - " " backgr. "

The numbers are shown as functions of the observed p_T^J .

For $p_T^J \gtrsim 1.5$ GeV/c, the number of correctly found jet particles is almost identical for the three methods (1.7-1.8, i.e. about 35% of the total number of generated particles), but the Principal Axis and G.S.2 methods pick up more background particles than the G.S.1 method, giving rise to a higher observed multiplicity in the jets. Because of this, in conjunction with the fixed p_T^J cut, these methods also lead to somewhat higher apparent efficiencies (fig. B1) than the G.S.1 method. For $p_T^J \lesssim 1.5$ GeV/c, in all three cases the output is seen to represent the original jet poorly, in the sense that more than 50% of the particles identified as jet particles are picked up from the background event.

The fact that the contribution to the found jets of particles coming from the background increases sharply for $p_T^J > 3$ GeV/c is due to the fixed input p_{xJ}^{MC} at 3 GeV/c.

The number of jet tracks lost is similar for all three methods (0.2-0.3).

It is concluded that a cut $p_T^J > 1.5$ GeV/c is necessary for the methods to work sensibly, so that the output jets represent the Monte Carlo input jets reasonably well.

The jet acceptance, ε , for Monte Carlo generated jets, is defined as

$$\varepsilon = \frac{\text{number of jet events found}}{\text{number of jet events generated}} \qquad \text{(B1)}$$

In the following ε is studied as a function of the parameters of the jet, for the three cases.

Fig. B3 shows ε as a function of the x-component of the input jet momentum, p_{xJ}^{MC} . The jets were generated with Gaussian distributions in y and ϕ , with widths as indicated on the figure.

For comparison, we also define the fraction of "findable" jets as the fraction of generated jets which satisfy the requirement $p_T^J > 1.5$ GeV/c after loss of neutrals, and application of acceptance cuts.

ε is seen to increase rapidly with p_{xJ}^{MC} , reaching values around 0.5 at $p_{xJ}^{MC} \approx 4$ GeV/c. For the G.S.2 and PA methods ε is somewhat bigger than for the G.S.1 method, as expected. The results of the G.S.1 method which has the most narrow set of smearing widths ($S_y = 0.5$, $S_\phi = 30^o$) agree, however, more closely with the fraction of findable jets. The larger values of ε for the G.S.2 method, and the PA method, must then be due to a larger pick-up of background by these methods.

The close agreement between ε and the fraction of findable jets does not mean that all findable jets are found. A few per cent are lost, but this is compensated by "non-findable" jets helped by background.

In fig. B4, ε is shown as a function of the rapidity, y_J , of the found jet. The jet azimuth, ϕ_J^{MC} , has been given a flat distribution in the range $|\phi_J^{MC}| < 30^o$, and p_{xJ}^{MC} has been kept fixed at 3 GeV/c.

In all cases ε is seen to be reasonably high and slowly varying for y_J^{MC} smaller than ~ 2 , after which a sharper drop is observed.

The results of the application of the Gaussian Smearing method with the small widths, G.S.1, are again seen to give the best agreement with the fraction of findable jets, although some difference in shape is observed between the two distributions.

It is thus concluded that where the methods are applicable, for $p_T^J > 1.5$ GeV/c, there are no compelling differences between them. The Gaussian Smearing method with the narrow set of widths, being the more restrictive, is, however, marginally better in representing the input.

In order to illustrate the bias imposed on the structure of the jets found by the Gaussian Smearing method we now turn to high p_T events in which a jet was found by this method.

Fig. B5 shows the distribution of rapidity distance, $\Delta y = |y-y_J|$, from the jet axis for particles classified as jet an non-jet particles, and for all AWAY side particles. The Gaussian Smearing method was used with the narrow set of smearing widths S_y, S_ϕ (G.S.1). Also shown is an uncorrelated distribution, obtained by placing the same distribution of jet axes in other high p_T events (with or without a jet).

The sharp spike at $\Delta y = 0$ in the distribution of all AWAY side particles is almost entirely due to particles classified as jet particles. A more detailed study shows, however, that the width, $\langle \Delta y \rangle$, of the distribution of Δy of the jet particles is simply proportional to the smearing width, S_y, used in the analysis. Therefore no physical interpretation should be given to the strength and width of this spike.

As the background distribution is seen to follow closely the distribution of all AWAY side particles at large Δy, where most of the particles are non-jet particles, it has been normalized to the same area in the region $\Delta y > 1$. The

deviation between this background and the distribution of non-jet particles around $\Delta y = 0$ can then be used to estimate the amount of background assigned to the jets. In this way one arrives at a number of ~ 0.5 particles, in good agreement with the Monte Carlo study above (see fig. B2).

REFERENCES

(1) M. Jacob and P.V. Landshoff, Phys. Rep. 48 (1978) 285.

(2) Symposium on "Jets in High Energy Collisions", Copenhagen, July 1978, Physica Scripta, 19 (1979) 69.

(3) G. Hanson, 7th International Colloquium on Multiparticle Reactions, Tutzing 1976.

(4) W. Scott, in (2).

(5) P. Darriulat, P. Dittman, K. Eggert, M. Holder, K.T. McDonald, T. Modis, F.L. Navarria, A. Seiden, J. Strauss, G. Vesztergombi and E.G.H. Williams, Nuclear Phys. B107 (1976) 429.

(6) M. Della Negra, D. Drijard, H.G. Fischer, G. Fontaine, H. Frehse, P. Frenkiel C. Ghesquiere, R. Gokieli, P. Hanke, W. Hofmann, P.G. Innocenti, W. Isenbeck, E.E. Kluge, V. Korbel, D. Linglin, A. Minten, A. Norton, A. Putzer, G. Sajot, R. Sosnowski, S. Stein, J. Stiewe, H.D. Wahl and D. Wegener, Nuclear Phys. B127 (1977) 1.

(7) M. Della Negra, D. Drijard, H.G. Fischer, G. Fontaine, H. Frehse, P. Frenkiel, G. Ghesquiere, R. Gokieli, P. Hanke, P.G. Innocenti, W. Isenbeck, E.E. Kluge, V. Korbel, S. Krzywdzinski, D. Linglin, A. Minten, D.R.O. Morrison, A. Putzer, H. Schneider, R. Stroynowski, S. Stein, W.J. Schwille and D. Wegener, Phys. Letters 59B (1975) 401.

(8) C. Bromberg, G. Fox, R. Gomez, J. Pine, S. Stampke, K. Yung, S. Erhan, E. Lorenz, M. Medinnis, J. Rohlf, P. Schlein, V. Ashford, H. Haggerty, R. Juhala, E. Malamud, S. Mori, R. Abrams, R. Delzenero, H. Goldberg, S. Margulies, D. McLeod, J. Solomon, R. Stanek, A. Dzierba and W. Kropac, Phys. Rev. Letters 38 (1977) 1447 and FERMILAB-Conf-77/62-Exp.

(9) M.G. Albrow, S. Almehed, P.S.L. Booth, X. de Bouard, H. Bøggild, L.J. Carroll, P. Catz, E. Dahl-Jensen, I. Dahl-Jensen, G. Damgaard, G. von Dardel, M. Davidson, N. Elverhaug, B. Guillerminet, K.H. Hansen, P. Hersleb, J.E. Hooper, J.N. Jackson, G. Jancso, G. Jarlskog, H.B. Jensen, L. Jönsson, A. Klovning, E. Lillethun, E. Lohse, A. Lu, B. Lörstad, N.A. McCubbin, H.E. Miettinen, J.V. Morris, R. Møller, S.Ø. Nielsen, J.O. Petersen, J.A.J. Skard, D.B. Smith and P. Villeneuve, Nuclear Phys. B135 (1978) 461.

(10) M.G. Albrow, S. Almehed, P.S.L. Booth, X. de Bouard, H. Bøggild, L.J. Carroll, P. Catz, E. Dahl-Jensen, I. Dahl-Jensen, G. Damgaard, G. von Dardel, N. Elverhaug, K.H. Hansen, J.N. Jackson, G. Jancso, G. Jarlskog, H.B. Jensen, L. Jönsson, A. Klovning, E. Lillethun, A. Lu, B. Lörstad, N.A. McCubbin, H.E. Miettinen, J.V. Morris, R. Møller, S.Ø. Nielsen, J.O. Petersen, J.A.J. Skard and P. Villeneuve, Nuclear Phys. B145 (1978) 305.

(11) B. Alper, H. Bøggild, P. Booth, F. Bulos, L.J. Carroll, G. Damgaard, G. von Dardel, B. Duff, K.H. Hansen, F. Heymann, J.N. Jackson, G. Jarlskog, L. Jönsson, A. Klovning, L. Leistam, E. Lillethun, E. Lohse, G. Lynch, G. Manning, K. Potter, M. Prentice, P. Sharp, S. Sharrock, S. Ølgaard-Nielsen, D. Quarrie and J.M. Weiss, Nuclear Phys. B100 (1975) 237.

(12) P. Capiluppi, G. Giacomelli, A.M. Rossi, G. Vannini, A. Bertin, A. Bussiere and R.J. Ellis, Nuclear Phys. B79 (1974) 189.

(13) A.M. Rossi, G. Vannini, A. Bussiere, E. Albini, D. D'Alessandro and G. Giacomelli, Nuclear Phys. B84 (1979) 269.

(14) M.G. Albrow, A. Bagchus, D.P. Barber, A. Bogaerts, B. Bosnjaković, J.R. Brooks, A.B. Clegg, F.C. Erné, C.N.P. Gee, D.H. Locke, F.K. Loebinger, P.G. Murphy, A. Rudge, J.C. Sens and F. van der Veen, Nuclear Phys. B56 (1973) 333 and Nuclear Phys. B73 (1974) 40.

(15) D. Antreasyan, J.W. Cronin, H.J. Frisch, M.J. Schochet, L. Kluberg, P.A. Piroué and R.L. Sumner, Phys. Rev. Letters 38 (1977) 112 and 115.

(16) Ch. Berger, W. Lackas, F. Raupach, W. Wagner, G. Alexander, L. Criegee, H.C. Dehne, K. Derikum, R. Devenish, G. Flügge, G. Franke, Ch. Gerke, E. Hackmack, P. Harms, G. Horlitz, Th. Kahl, G. Knies, E. Lehmann, B. Neumann, R.L. Thompson, U. Timm, P. Waloschek, C.G. Winter, S. Wolff, W. Zimmermann, O. Achterberg, V. Blobel, L. Boesten, H. Daumann, A.F. Garfinkel, H. Kapitza, B. Koppitz, W. Lührsen, R. Maschuw, H. Spitzer, R. van Staa, G. Wetjen, A. Bäcker, S. Brandt, J. Bürger, C. Grupen, H.J. Meyer, G. Zech, H.J. Daum, H. Meyer, O. Meyer, M. Rössler and K. Wacker, Phys. Letters B78 (1978) 176 and DESY preprint Nov. 1978, submitted to Phys. Letters.

(17) G. Hanson, 13th Rencontre de Moriond, Les Arcs, Savoie, France, March 1978.

(18) J. Bell, C.T. Coffin, R.N. Diamond, H.T. French, W.C. Louis, B.P. Roe, R.T. Ross, A.A. Seidl, J.C. Vander Velde, E. Wang, J.P. Berge, D.V. Bogert, F.A. DiBianca, R. Endorf, R. Hanft, C. Kochowski, J.A. Malko, G.I. Moffatt, F.A. Nezrick, W.G. Scott, W. Smart, R.J. Cence, F.A. Harris, M. Jones, M.W. Peters, V.Z. Peterson, V.J. Stenger, G.R. Lynch, J.P. Marriner and M.L. Stevenson, Phys. Rev. D19 (1979) 1.

(19) R.P. Feynman, R.D. Field and G.C. Fox, Phys. Rev. D18 (1978) 3320.

(20) H. Bøggild, 14th Rencontre de Moriond, Les Arcs, Savoie, France, March 1979, Niels Bohr Institute preprint NBI-HE-79-6.

(21) The model is very simplified. In particular the fragmentation function (A3) used is non-scaling, and cannot be expected to hold over a wide range of jet momenta. We have however found that it is adequate for the purposes of the present paper.

Table 1

Data samples used ($\sqrt{s}$ = 52.6 GeV).

p_{TRIG} (GeV/c)	$< p_{TRIG} >$ (GeV/c)	Events
0.5 - 1.5	1.1	46401
1.5 - 2.5	1.9	30944
2.5 - 3.5	2.9	17184
3.5 - 4.5	3.8	2219
4.5 - 6.0	4.9	263
Total	1.8	97011
Min. Bias		23340

FIGURE CAPTIONS

Fig. 1: Schematic plan view of the apparatus. The beams intersect in the vacuum chamber inside the Split Field Magnet (SFM). In the Wide Angle Spectrometer (WAS) BM is a bending magnet, SC1-SC5 are spark chambers, 1H-4H and 2V-4V are horizontal and vertical scintillator hodoscopes, respectively, and $\check{C}1$-$\check{C}2$ are gas Čerenkov counters. The coordinate system used is also shown (displaced).

Fig. 2: Calculated AWAY side acceptance for particles with $\Delta p/p < 0.5$, at $\sqrt{s} = 52.6$ GeV, shown as a function of y, in two bins of $|\phi|$ and three bins of p_T, for positive and negative particles respectively.

Fig. 3: Distribution of rapidity difference, Δy, between pairs of AWAY side particles with $p_T > p_T^o$, for $2.5 < p_{TRIG} < 6.0$ GeV/c, and for three values of p_T^o. The figure shows:

a) neutral pairs, and
b) doubly charged pairs.

Also shown (in full line) are distributions obtained by taking pairs of particles from different events.

Fig. 4: Signal for pairs of AWAY side particles with $p_T > p_T^o$ and $\Delta y < 1$, as a function of p_T^o. The average value of p_{TRIG} is 3.0 GeV/c.

Fig. 5: $\langle \Delta y \rangle$ inside $\Delta y < 1$ for pairs of AWAY side particles with $p_T > p_T^o$, as a function of p_T^o. $\langle \Delta y \rangle$ was calculated from the Δy distributions with a background subtracted. The dashed line shows the result of a model calculation (see text).

Fig. 6: Distribution of invariant mass, M , of pairs of AWAY side particles (taken to be pions), with $p_T > p_T^o$, for $2.5 < p_{TRIG} < 6.0$ GeV/c, and for three values of p_T^o . The figure shows a) neutral pairs, and b) doubly charged pairs. A background has been subtracted, normalized to the region $\Delta y > 1$.

Fig. 7: Example of an event analysed by the Gaussian Smearing method. The figure shows:

a) The event represented by the x-y projection of the momentum vectors of the reconstructed tracks. The trigger momentum is 9 GeV/c.

b) Graph of the density function $G(y, \phi)$ of transverse momentum on the AWAY side. The maximum is at 5.4 GeV/c.

c) Contour plot of $G(y, \phi)$.
_____ shows 1 GeV/c intervals,
__ . __ shows 0.2 GeV/c intervals,
_ _ _ represents the level curve at half the peak height.

Fig. 8: Fraction of events containing an AWAY side jet. The Gaussian Smearing method with $(S_y , S_\phi) = (0.5 , 30^o)$ has been used.

The point marked by an open circle was obtained from Minimum Bias events, requiring a "trigger" particle in the region $|y| < 1$, $|180^o - \phi| < 30^o$ (around the direction of the WAS).

The point at $p_{TRIG} = 0$ shows the frequency of (AWAY side) jets in Minimum Bias events.

The lines show the results of Monte Carlo simulations with $p_{xJ}^{MC} = p_{TRIG}$ (dashed) and $p_{xJ}^{MC} = p_{TRIG} - 0.8$ GeV/c (dashed-dotted).

Fig. 9: Distribution of rapidity, y_J , of the jet axis, for Minimum Bias events and for four intervals of p_{TRIG} . The lines show the result of a model calculation (see text).

Fig. 10: Distribution of azimuth, ϕ_J, of the jet axis, for Minimum Bias events and for four intervals of p_{TRIG}. A cut $|y_J| < 1$ has been applied. The lines show the result of a model calculation (see text).

Fig. 11: Observed and corrected widths, σ_y^J and σ_ϕ^J, from Gaussian fits to the distributions of jet rapidity and azimuth, as functions of p_{TRIG}. Also shown is the model input necessary to simulate the data. The crosses show the corresponding widths, σ_y, for single AWAY side particles with $p_T > 0.8$ GeV/c.

Fig. 12: $\frac{1}{N_{TRIG}} \cdot \frac{1}{p_T^J} \cdot \frac{dn}{dp_T^J}$ as a function of p_T^J, for Minimum Bias events and for four intervals of p_{TRIG}. The jet axis has been restricted to the region $|y_J| < 1$, $|\phi_J| < 30^\circ$. The lines show the results of a model calculation (see text).

Fig. 13: Observed and corrected slope, a, from exponential fits to $\frac{1}{N_{TRIG}} \cdot \frac{1}{p_T^J} \cdot \frac{dn}{dp_T^J}$ in the range $1.5 < p_T^J$ 4 GeV/c.

Fig. 14: p_T^o and $< p_T^J >$ corresponding to one AWAY side jet per event as functions of p_{TRIG}.

Fig. 15: Observed and corrected charged multiplicity, $< n_{ch}^J >$, in the jets as functions of p_{TRIG}. The corrections assumes an exponential z-distribution. Data from e^+e^- annihilations (16, 17) are also shown.

Fig. 16: Distribution of the fractional longitudinal momentum, z, with respect to the observed jet momentum, of the jet particles in four intervals of p_{TRIG}. The line shows the result of a model calculation corresponding to $2.5 < p_{TRIG} < 3.5$ GeV/c.

Fig. 17: Observed and corrected slope, b , from exponential fits to the ζ -distribution in the interval $0.2 < \zeta < 0.8$. Also shown are the corresponding slopes of the $x_{\parallel}$ -distribution, where $x_{\parallel}$ is the longitudinal momentum divided by the jet energy. Slopes of the $x_{\parallel}$ -distributions in e^+e^- jets and jets from νp collisions are also shown.

Fig. 18: Distribution of $x_{\parallel}$ corresponding to our corrected z-distributions at two values of p_{TRIG} , compared to $x_{\parallel}$ -distributions for e^+e^- jets at corresponding c.m. energies (17).

Fig. 19: Mean charge, $< Q_J >$, of the jets for the six trigger types. Only jet particles with $p_T > 0.3$ GeV/c have been used in forming Q_J .

Fig. 20: Average charge per observed jet particle as a function of ζ for positive and negative triggers, in two intervals of p_{TRIG} .

Fig. 21: Average charge per observed jet particle as a function of ζ for positive and negative jet leaders, in two intervals of ζ for the jet leader, ζ_{max}.

Fig. B1: Number of found jets per event, and mean deviations $< |y_J - y_J^{MC}| >$, $< |\phi - \phi_J^{MC}| >$ between found and Monte Carlo generated jet axes, as functions of the "observed" p_T^J for: P.A.: Principal Axis Method, G.S.1 and G.S.2: Gaussian Smearing method with $(S_y , S_\phi) = (0.5 , 30^\circ)$, and $(0.75 , 45^\circ)$, respectively.

Fig. B2: Number of charged particles, in the four categories Jj , Jb , Bj , Bb (J: found as jet particle, B: found as background particle, j: generated as jet particle, b: generated as background particle), for the two jet analysis methods, as functions of the "observed" p_T^J . The numbers come from the analysis of model events.

Fig. B3: Jet acceptance $\mathcal{E}$ = number of jet events found/number of model jet events generated, as a function of p_{xJ}^{MC}, for the Principal Axis method, and for the Gaussian Smearing method with widths $(S_y, S_\phi) = (0.5, 30^o)$ (G.S.1), and $(0.75, 45^o)$ (G.S.2). Also shown is the fraction of "findable" jets (see text).

Fig. B4: Jet acceptance $\mathcal{E}$, as a function of y_J^{MC}, for the Principal Axis method, and for Gaussian Smearing with widths $(S_y, S_\phi) = (0.5, 30^o)$ (G.S.1), and $(0.75, 45^o)$ (G.S.2). Also shown is the fraction of "findable" jets (see text).

Fig. B5: Distribution of rapidity distance $\Delta y = |y-y_J|$ from the jet axis for all AWAY side particles, jet particles and non-jet particles in high p_T triggered events. The G.S.1 method has been used. Also shown is an uncorrelated distribution.

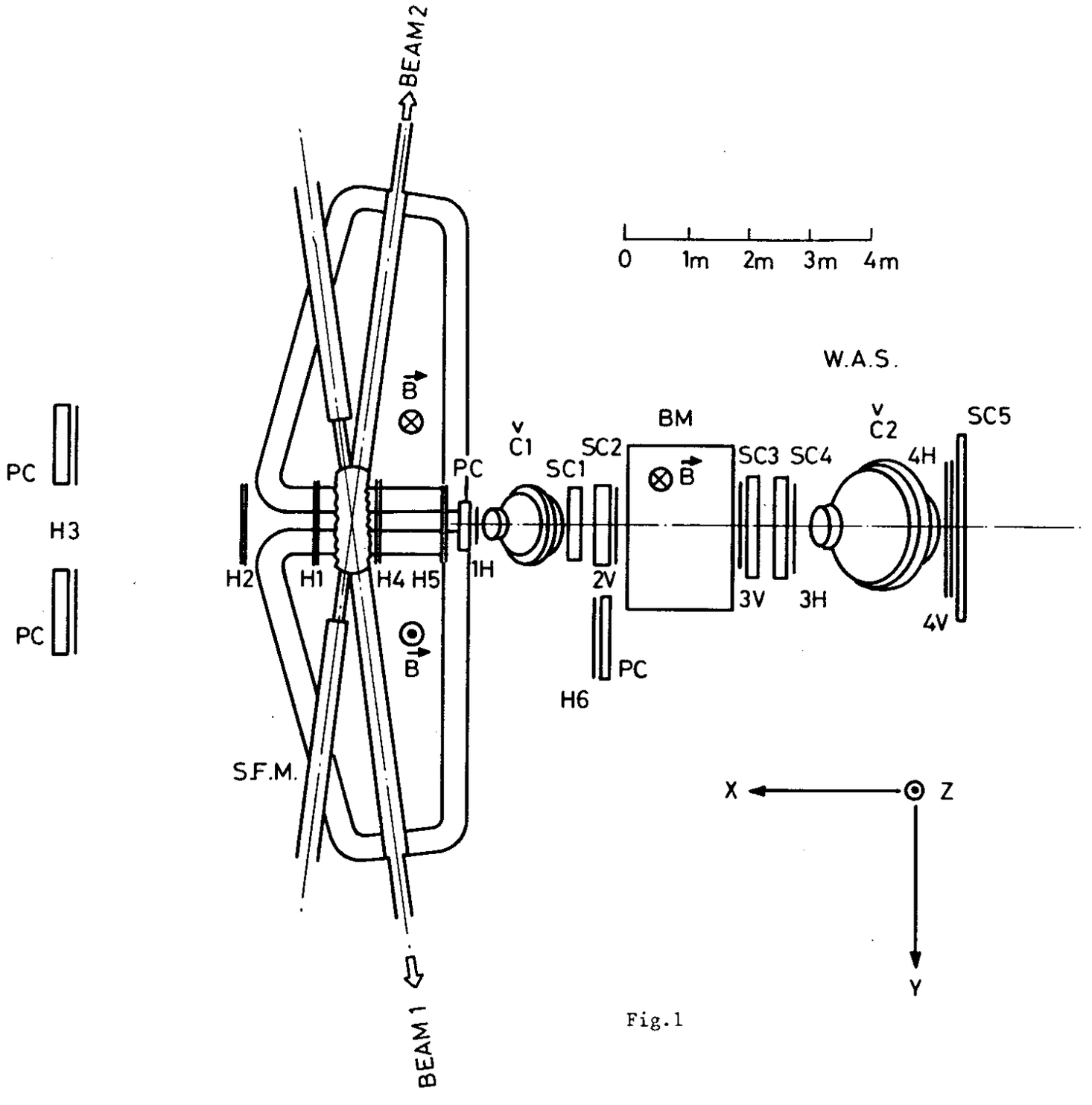
BEAM 2
0
1m
2m
3m
4m
W.A.S.
PC
H3
PC
B
PC
C1
SC1
SC2
BM
B
SC3
SC4
C2
4H
SC5
H2
H1
H4
H5
1H
2V
3V
3H
4V
H6
PC
S.F.M.
B
X
Z
Y
BEAM 1

Fig.1

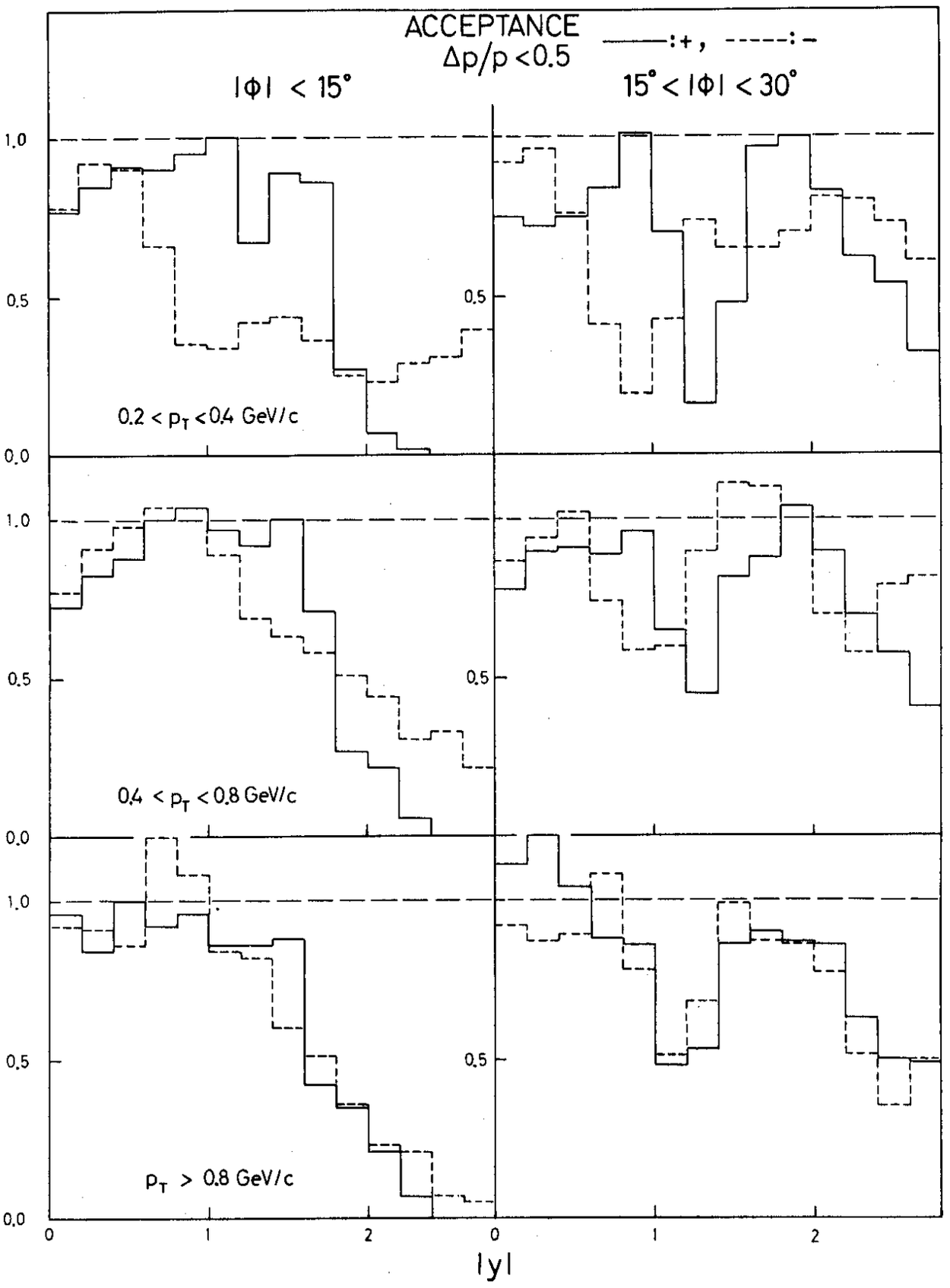
ACCEPTANCE
Δp/p <0.5
——:+, -----:-
|φ| < 15°
15° < |φ| < 30°
0.2 < p_T < 0.4 GeV/c
0.4 < p_T < 0.8 GeV/c
p_T > 0.8 GeV/c
1.0
0.5
0.0
0
1
2
|y|

Fig. 2

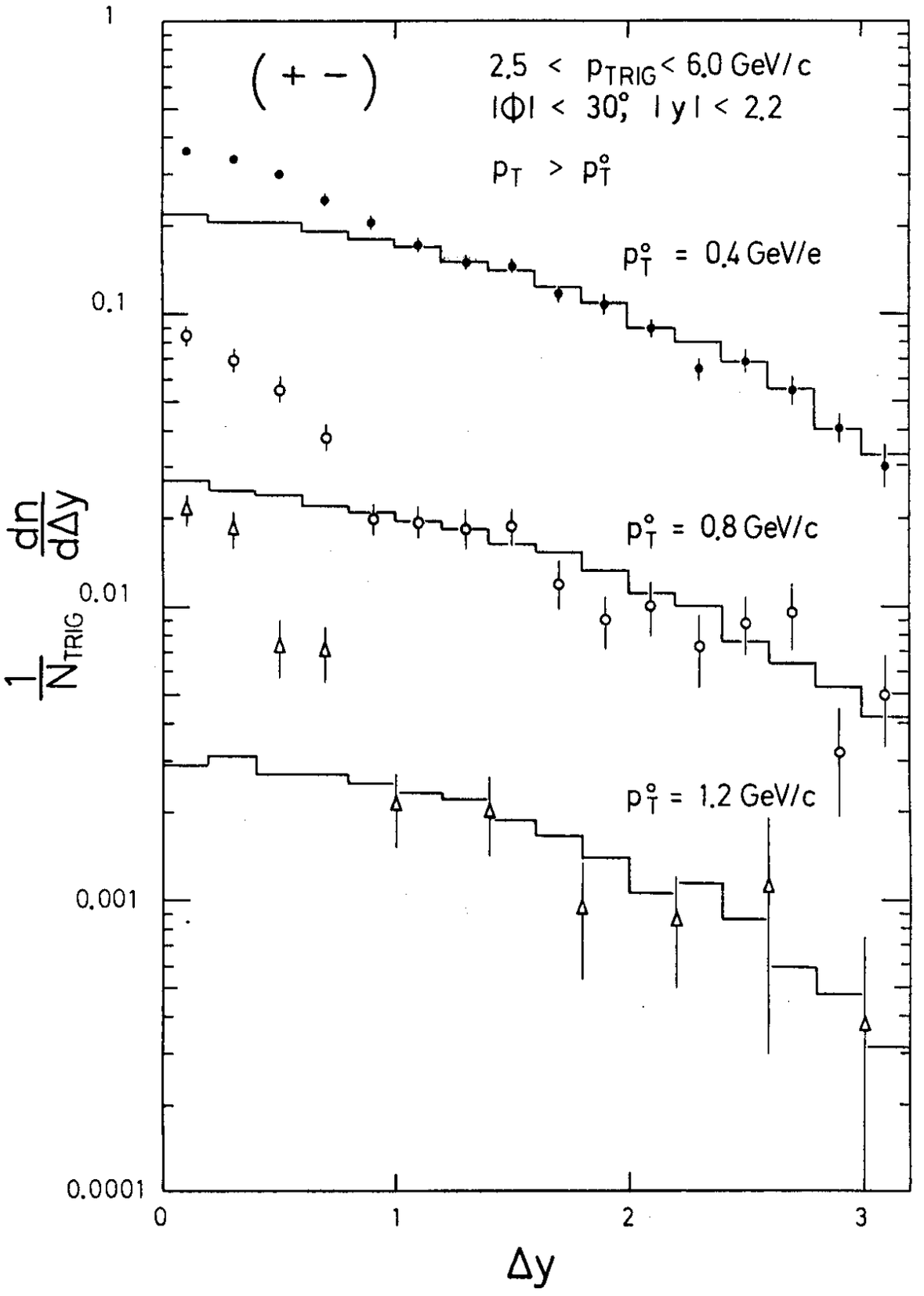
(+ −)
2.5 < p_{TRIG} < 6.0 GeV/c
|Φ| < 30°, |y| < 2.2
p_T > p_T°
p_T° = 0.4 GeV/c
p_T° = 0.8 GeV/c
p_T° = 1.2 GeV/c
$\frac{1}{N_{TRIG}} \frac{dn}{d\Delta y}$
1
0.1
0.01
0.001
0.0001
0
1
2
3
Δy

Fig. 3a

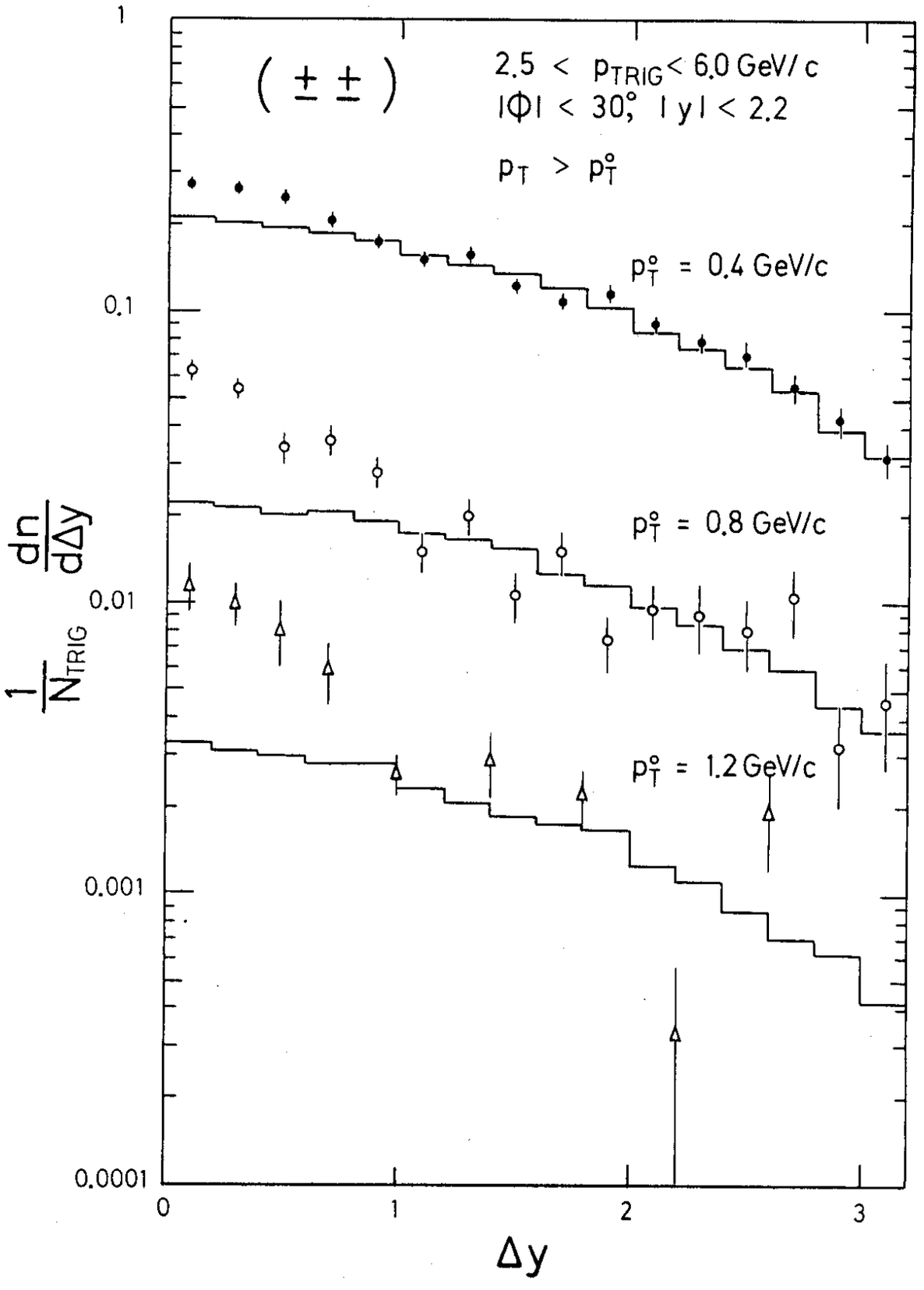
(± ±)
2.5 < pTRIG < 6.0 GeV/c
|Φ| < 30°, |y| < 2.2
pT > p°T
p°T = 0.4 GeV/c
p°T = 0.8 GeV/c
p°T = 1.2 GeV/c
1/NTRIG dn/dΔy
Δy
1
0.1
0.01
0.001
0.0001
0
1
2
3

Fig. 3b

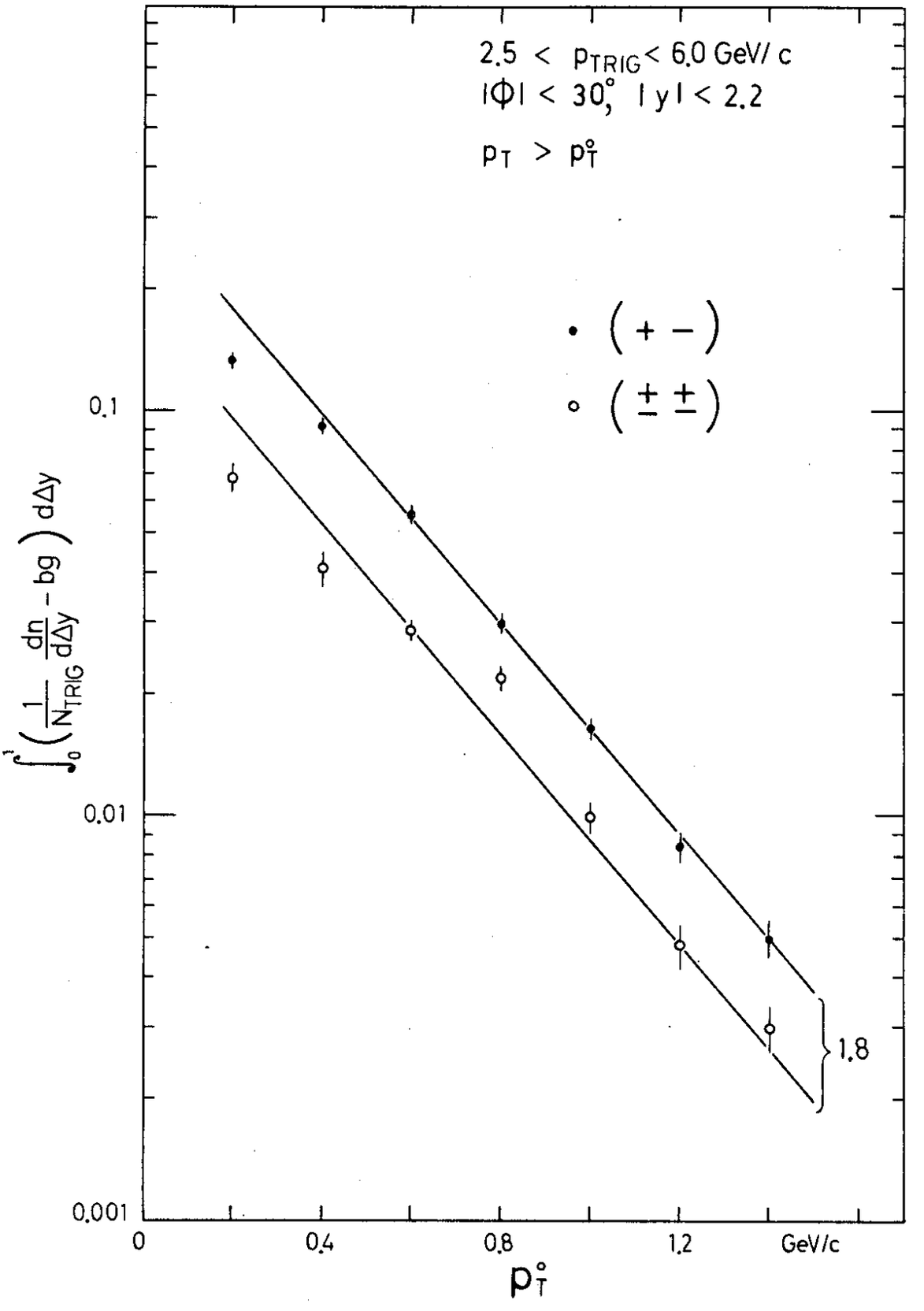
2.5 < p_{TRIG} < 6.0 GeV/c
|Φ| < 30°, |y| < 2.2
$p_T > p_T^\circ$
• (+ −)
○ (± ±)
$\int_0^1 \left(\frac{1}{N_{TRIG}} \frac{dn}{d\Delta y} - bg \right) d\Delta y$
0.1
0.01
0.001
1.8
0
0.4
0.8
1.2
GeV/c
p_T°

Fig. 4

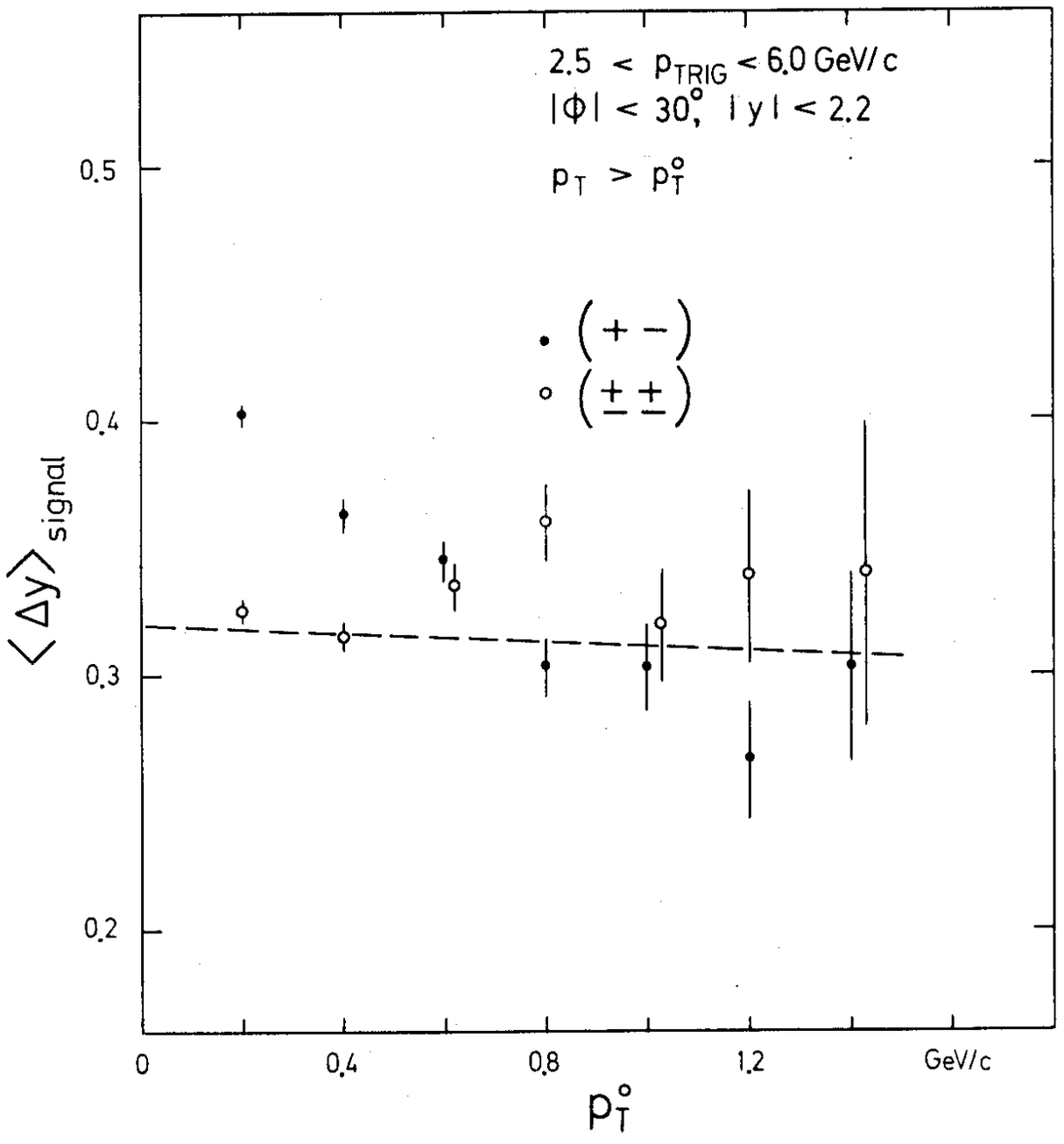
2.5 < p_TRIG < 6.0 GeV/c
|φ| < 30°, |y| < 2.2
p_T > p_T°
(+ −)
(± ±)
⟨Δy⟩ signal
0.5
0.4
0.3
0.2
0
0.4
0.8
1.2
GeV/c
p_T°

Fig. 5

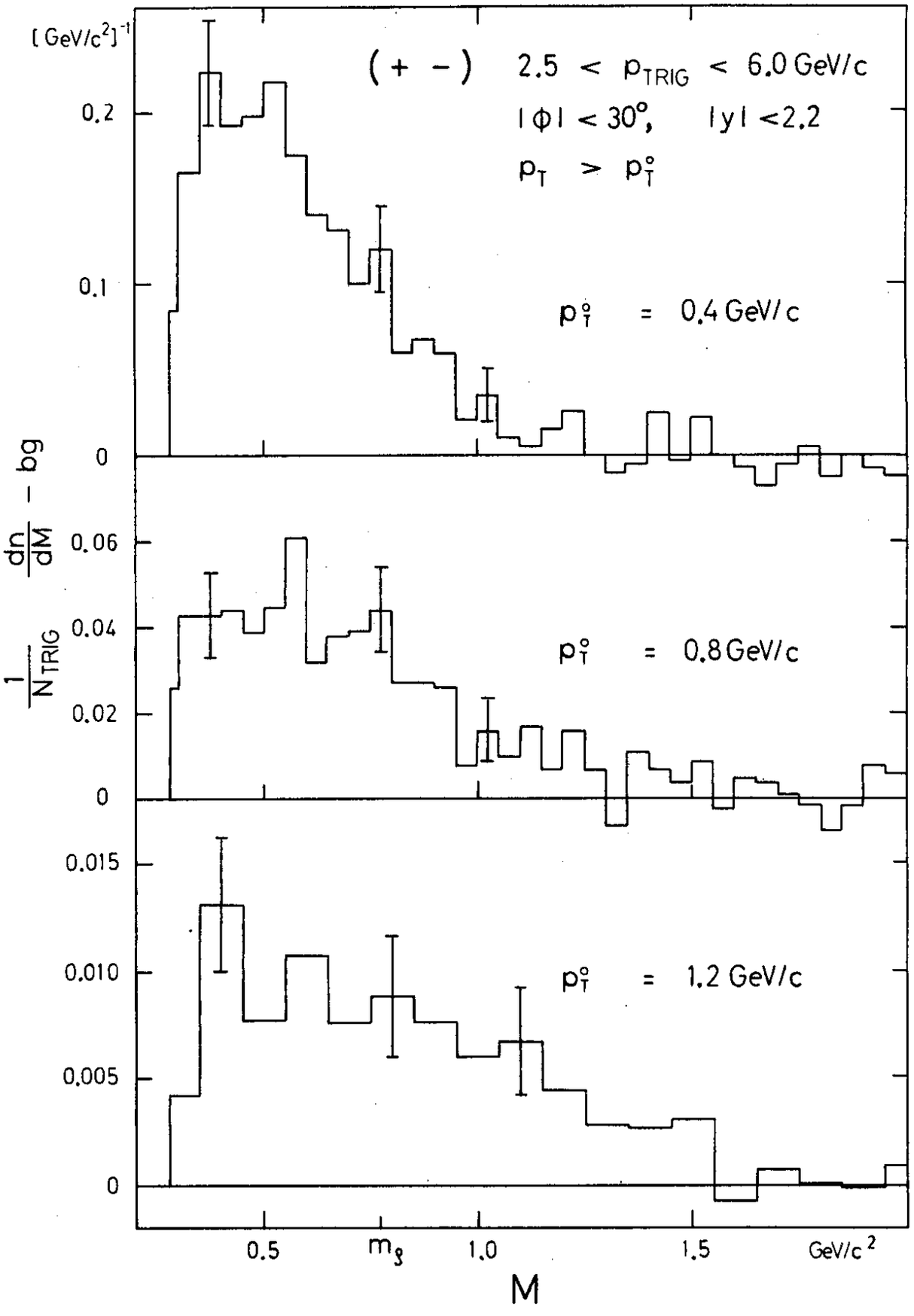
[GeV/c²]⁻¹
(+ −) 2.5 < p_TRIG < 6.0 GeV/c
|φ| < 30°, |y| < 2.2
p_T > p_T°
p_T° = 0.4 GeV/c
p_T° = 0.8 GeV/c
p_T° = 1.2 GeV/c
1/N_TRIG dn/dM − bg
0.2
0.1
0
0.06
0.04
0.02
0
0.015
0.010
0.005
0
0.5
m_g
1.0
1.5
GeV/c²
M

Fig. 6a

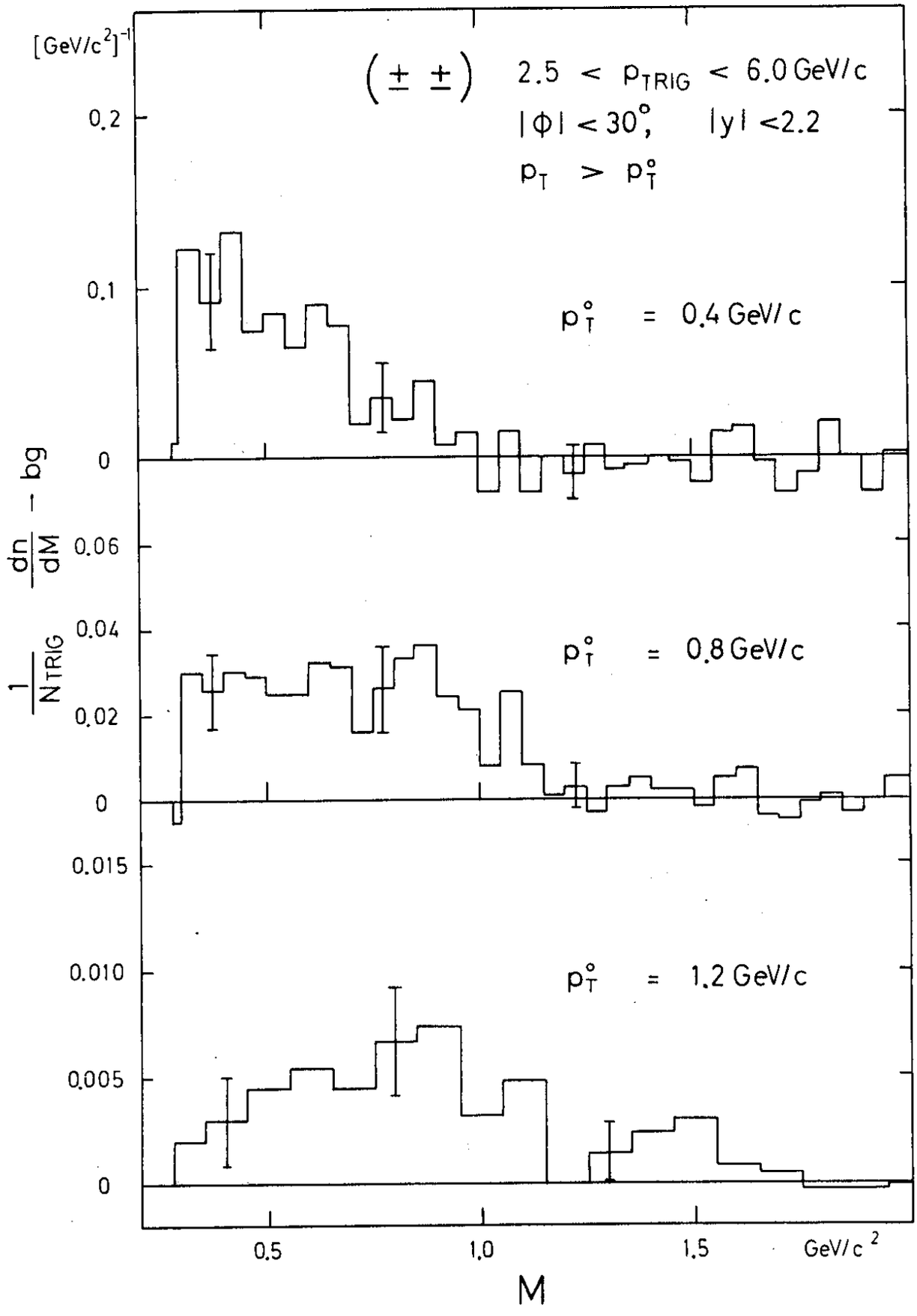
[GeV/c²]⁻¹
(± ±)
2.5 < p_TRIG < 6.0 GeV/c
|φ| < 30°, |y| < 2.2
p_T > p_T°
p_T° = 0.4 GeV/c
p_T° = 0.8 GeV/c
p_T° = 1.2 GeV/c
1/N_TRIG dn/dM − bg
M
GeV/c²
0.2
0.1
0
0.06
0.04
0.02
0
0.015
0.010
0.005
0
0.5
1.0
1.5

Fig. 6b

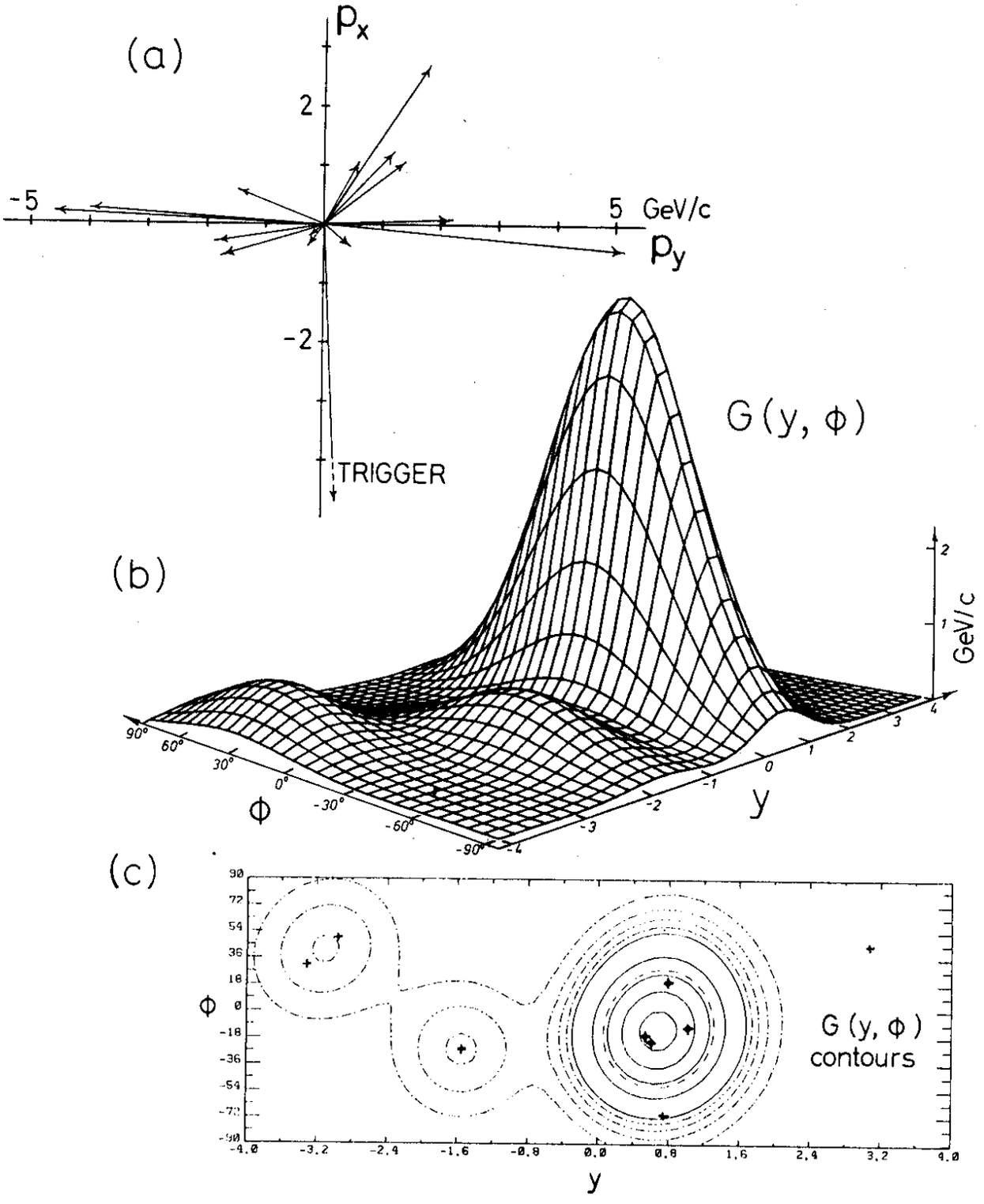

Fig. 7

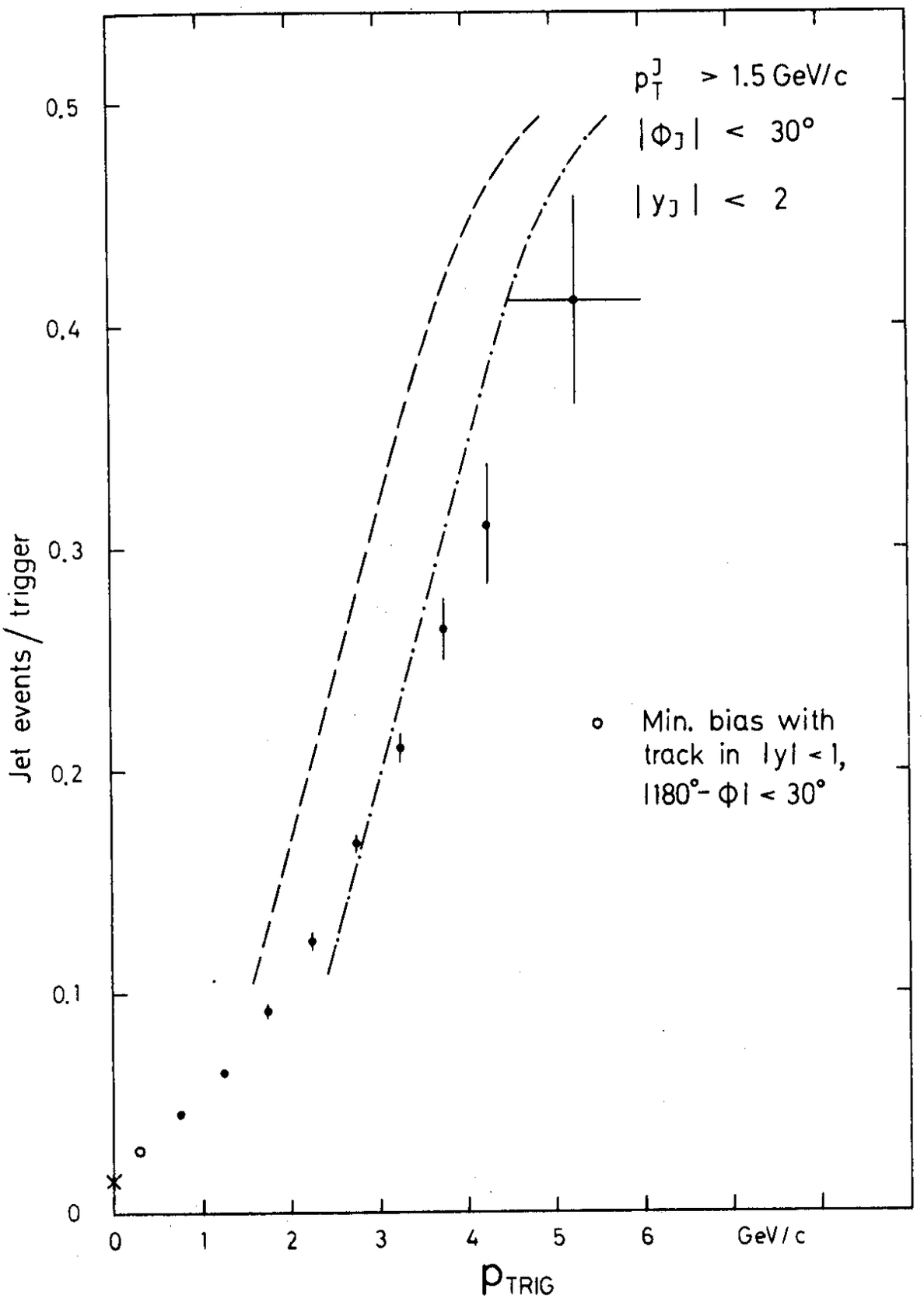
p_T^J > 1.5 GeV/c
$|\Phi_J|$ < 30°
$|y_J|$ < 2
o Min. bias with track in |y| < 1, |180°- Φ| < 30°
Jet events / trigger
0.5
0.4
0.3
0.2
0.1
0
0
1
2
3
4
5
6
GeV/c
p_{TRIG}

Fig. 8

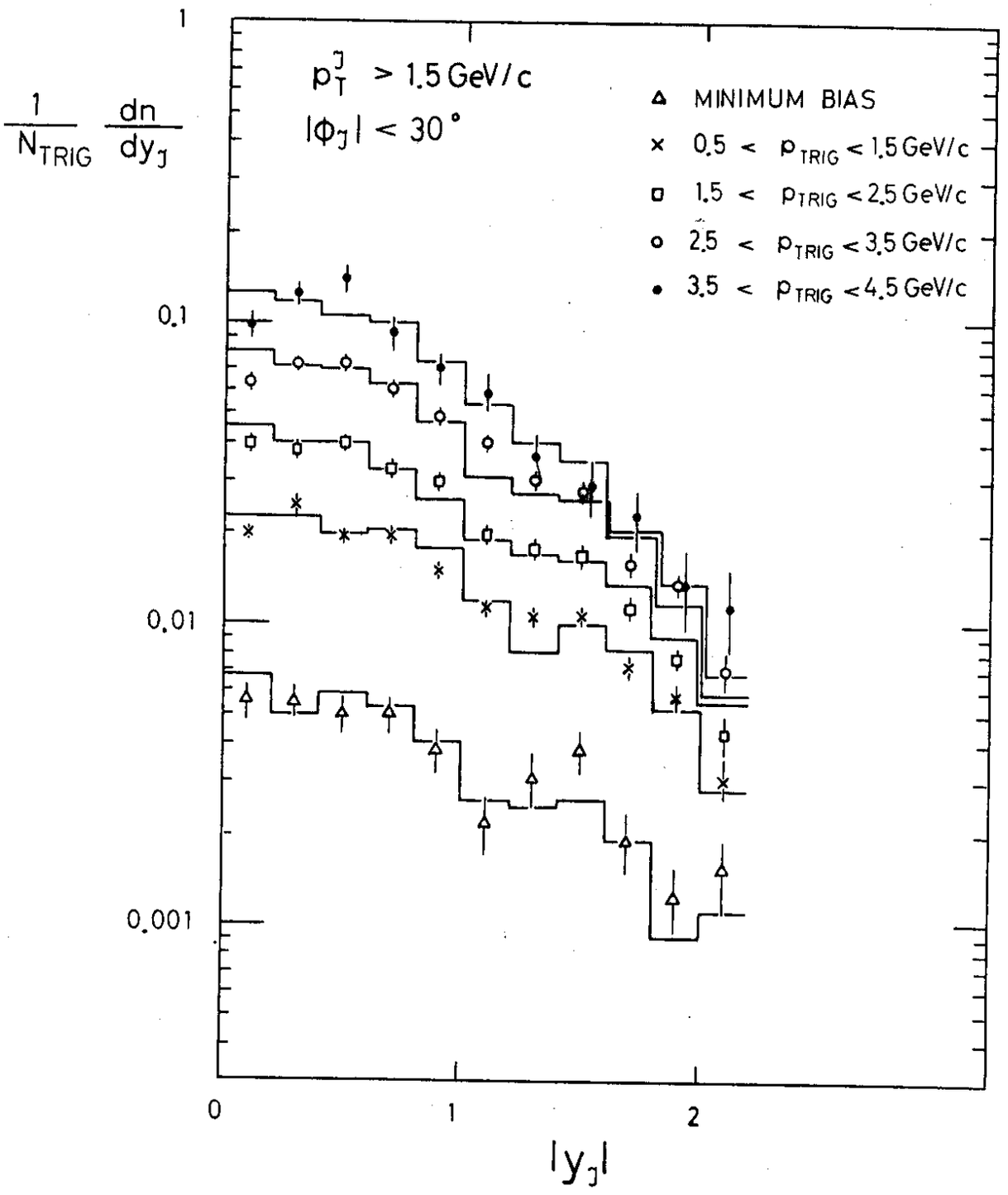
$\frac{1}{N_{TRIG}} \frac{dn}{dy_J}$
1
0.1
0.01
0.001
$p_T^J > 1.5$ GeV/c
$|\phi_J| < 30°$
MINIMUM BIAS
$0.5 < p_{TRIG} < 1.5$ GeV/c
$1.5 < p_{TRIG} < 2.5$ GeV/c
$2.5 < p_{TRIG} < 3.5$ GeV/c
$3.5 < p_{TRIG} < 4.5$ GeV/c
0
1
2
$|y_J|$

Fig. 9

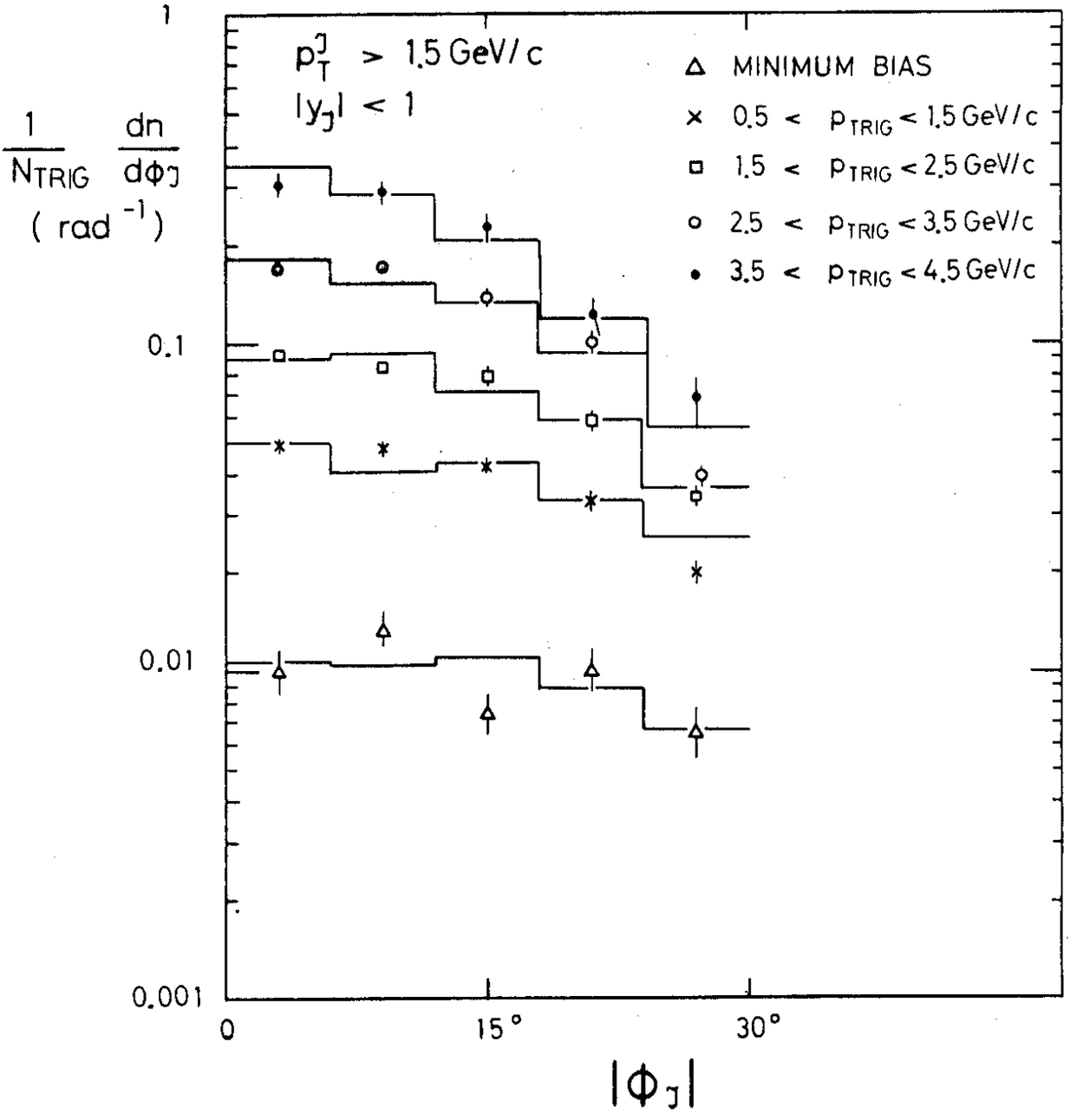
1
0.1
0.01
0.001
$\frac{1}{N_{TRIG}} \frac{dn}{d\phi_J}$
(rad $^{-1}$)
$p_T^J > 1.5$ GeV/c
$|y_J| < 1$
MINIMUM BIAS
$0.5 < p_{TRIG} < 1.5$ GeV/c
$1.5 < p_{TRIG} < 2.5$ GeV/c
$2.5 < p_{TRIG} < 3.5$ GeV/c
$3.5 < p_{TRIG} < 4.5$ GeV/c
0
15°
30°
$|\phi_J|$

Fig. 10

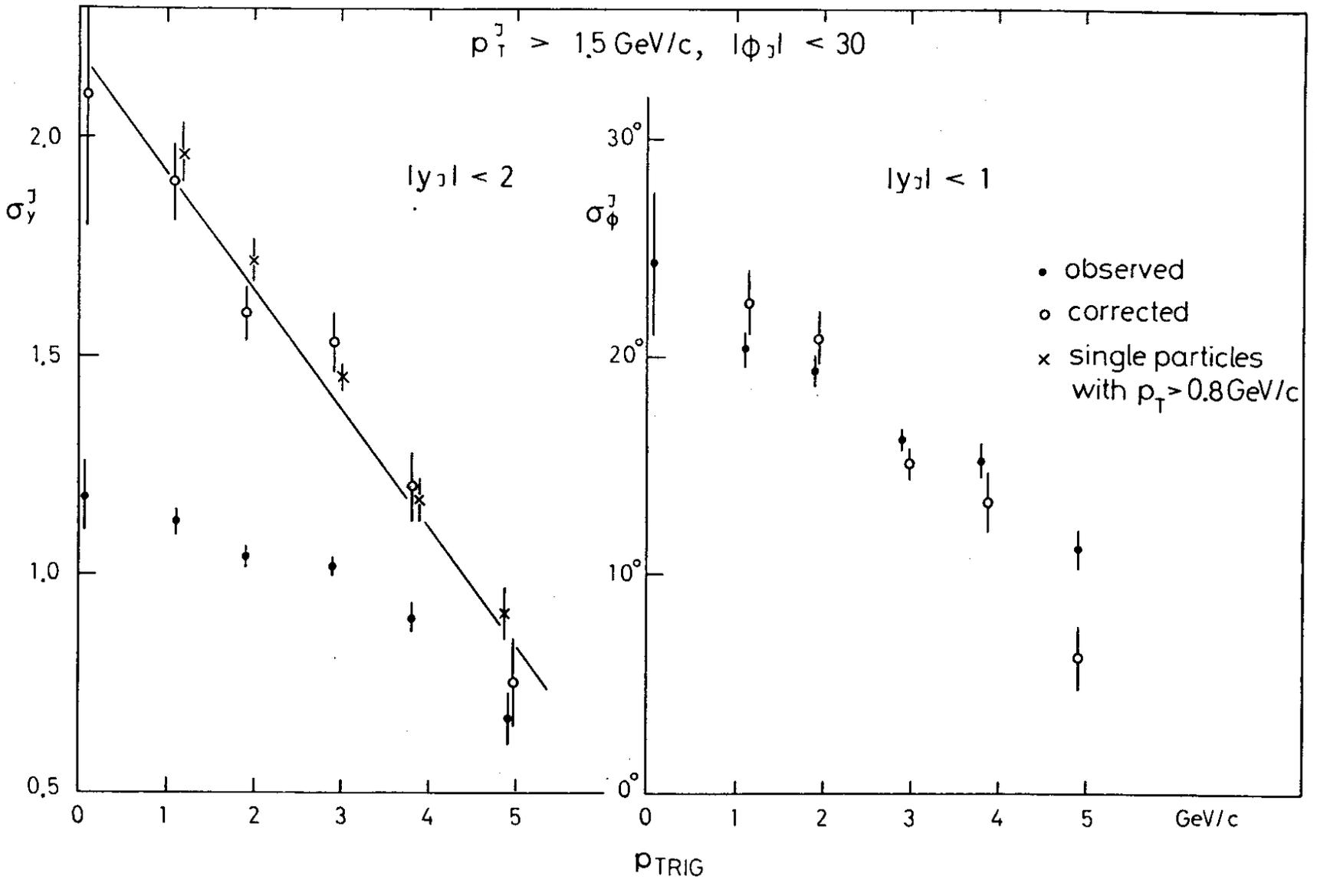
$p_T^J > 1.5$ GeV/c, $|\phi_J| < 30$
$|y_J| < 2$
$|y_J| < 1$
σ_y^J
σ_ϕ^J
2.0
1.5
1.0
0.5
30°
20°
10°
0°
0
1
2
3
4
5
GeV/c
p_{TRIG}
• observed
o corrected
× single particles with $p_T > 0.8$ GeV/c

Fig. 11

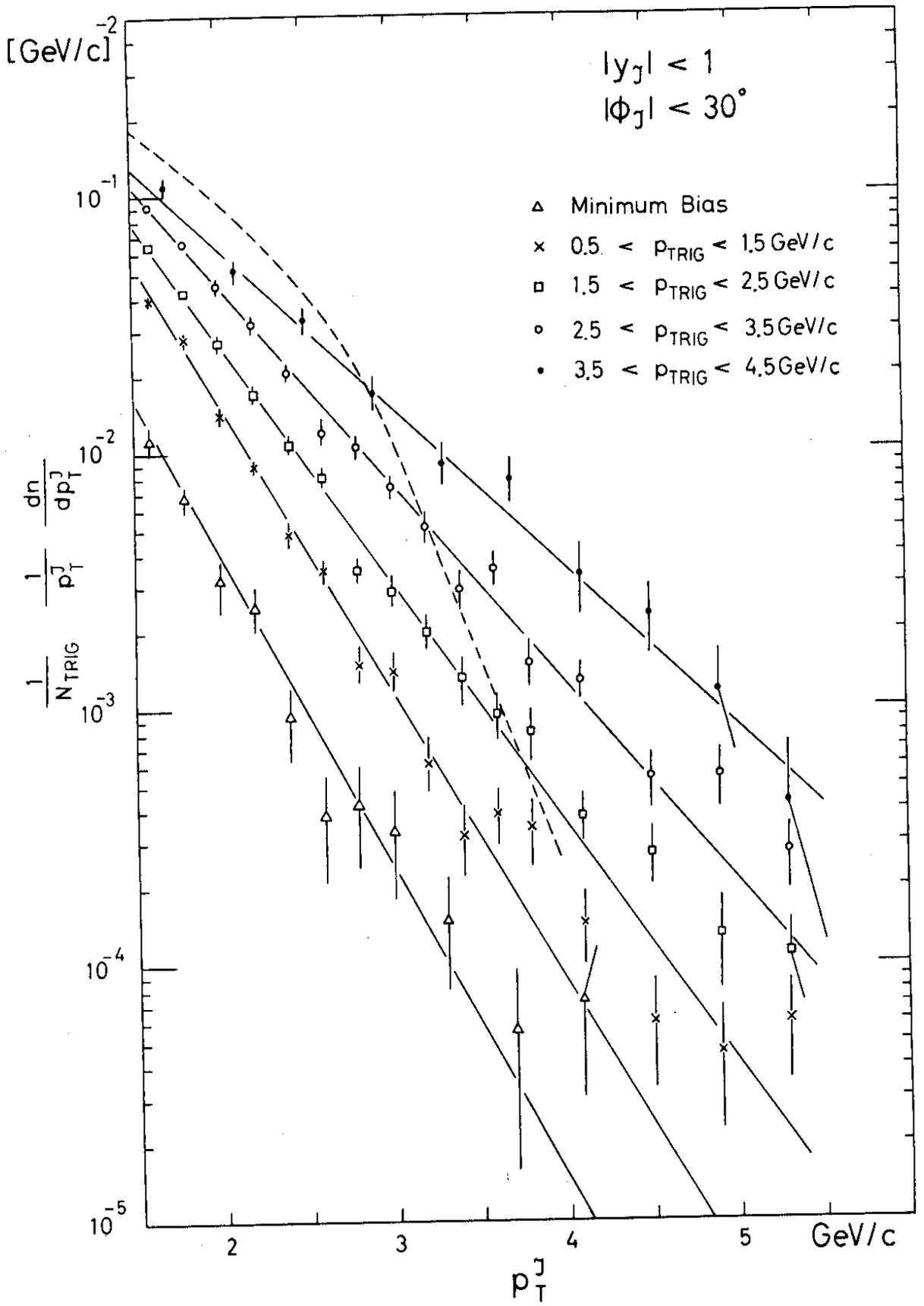
[GeV/c]$^{-2}$
$|y_J| < 1$
$|\phi_J| < 30°$
Minimum Bias
0.5 < p_{TRIG} < 1.5 GeV/c
1.5 < p_{TRIG} < 2.5 GeV/c
2.5 < p_{TRIG} < 3.5 GeV/c
3.5 < p_{TRIG} < 4.5 GeV/c
$\frac{1}{N_{TRIG}} \frac{1}{p_T^J} \frac{dn}{dp_T^J}$
10^{-1}
10^{-2}
10^{-3}
10^{-4}
10^{-5}
2
3
4
5
GeV/c
p_T^J

Fig. 12

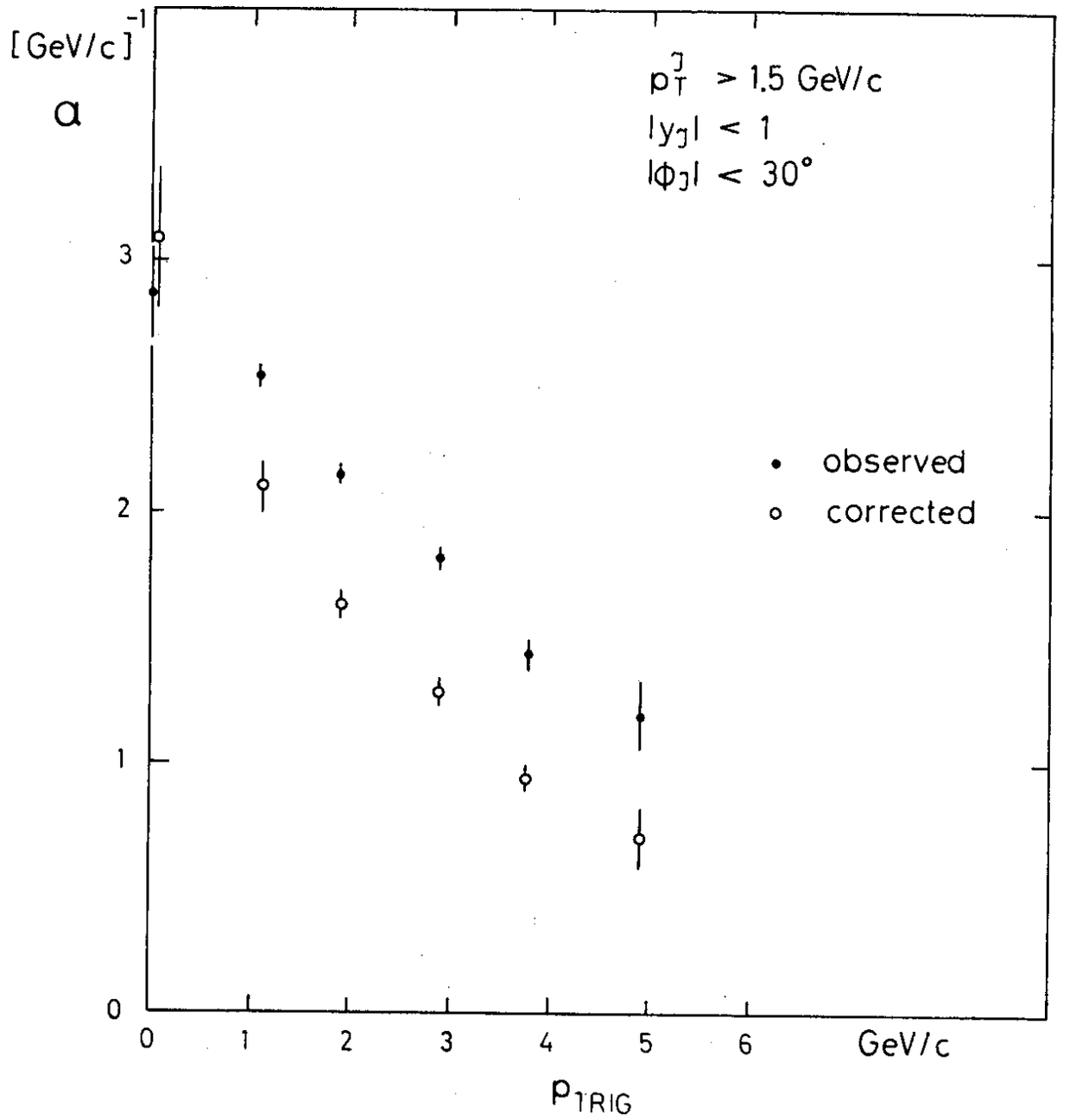
[GeV/c]$^{-1}$
a
p_T^J > 1.5 GeV/c
$|y_J|$ < 1
$|\phi_J|$ < 30°
observed
corrected
0
1
2
3
0
1
2
3
4
5
6
GeV/c
p_{TRIG}

Fig. 13

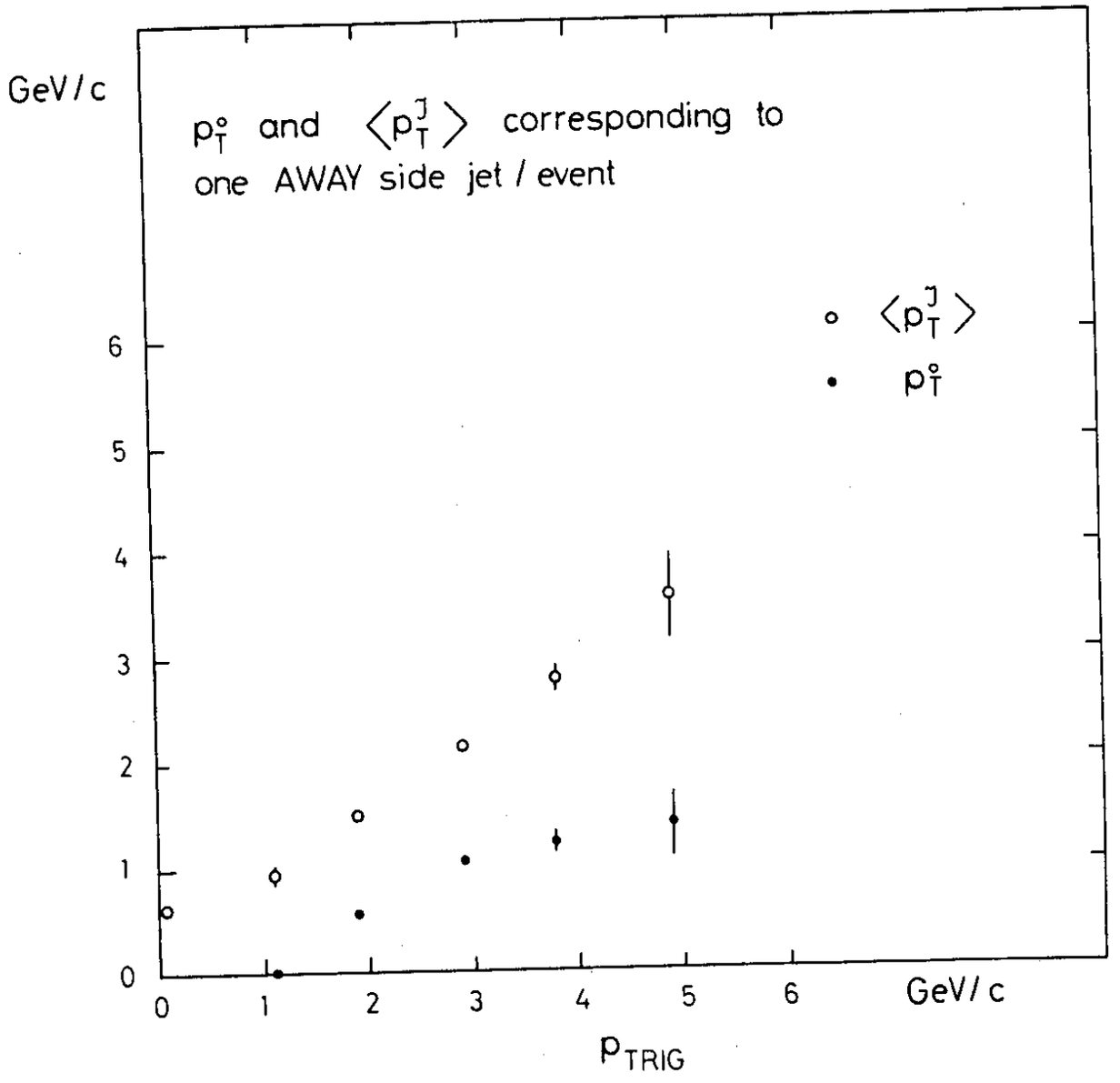
GeV/c
p_T° and $\langle p_T^J \rangle$ corresponding to
one AWAY side jet / event
$\langle p_T^J \rangle$
p_T°
0
1
2
3
4
5
6
GeV/c
p_{TRIG}

Fig. 14

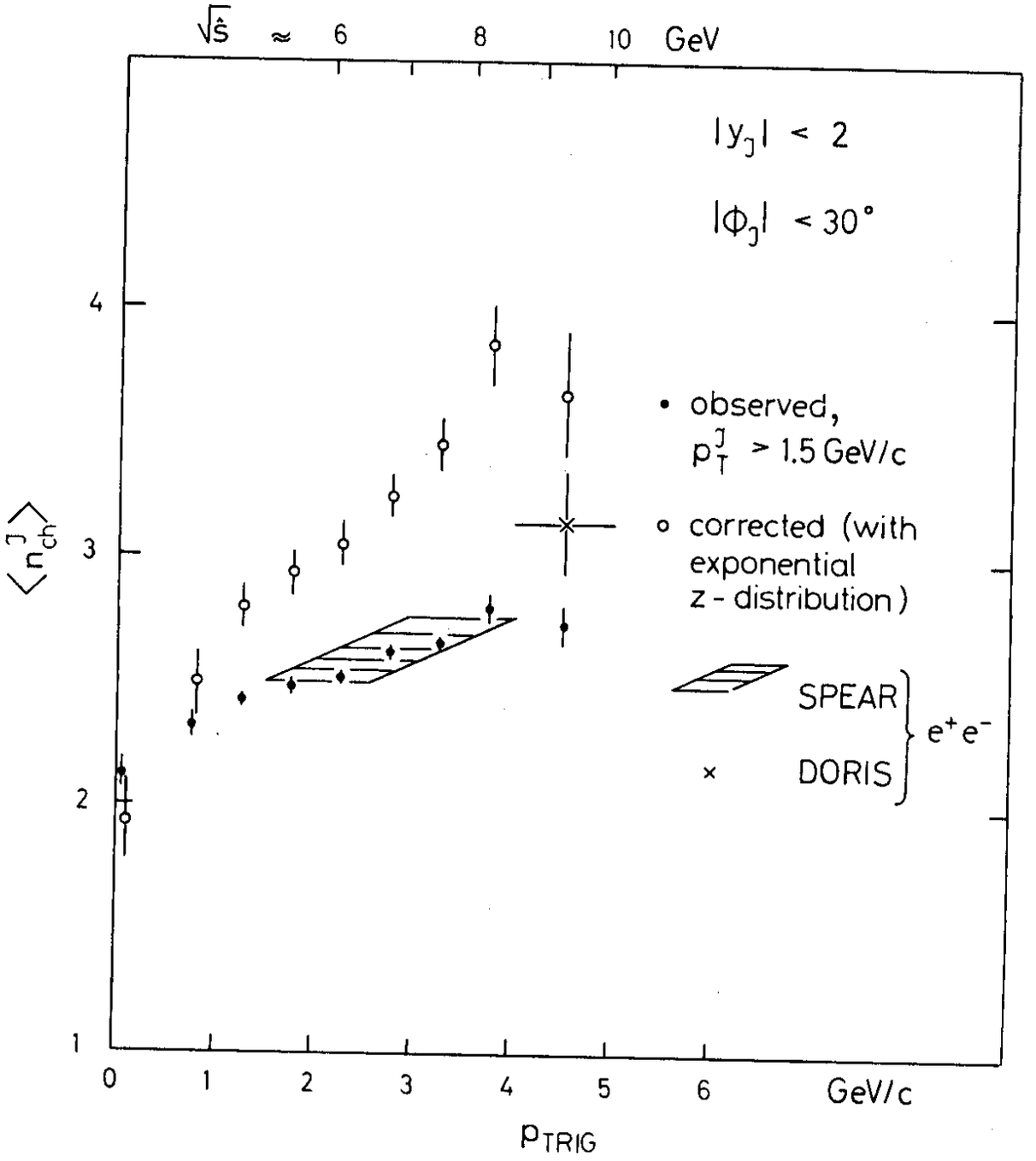
√ŝ ≈ 6 8 10 GeV
|y_J| < 2
|Φ_J| < 30°
• observed, p_T^J > 1.5 GeV/c
o corrected (with exponential z - distribution)
SPEAR
DORIS
e⁺e⁻
⟨n_ch^J⟩
p_TRIG
GeV/c
0 1 2 3 4 5 6
1 2 3 4

Fig. 15

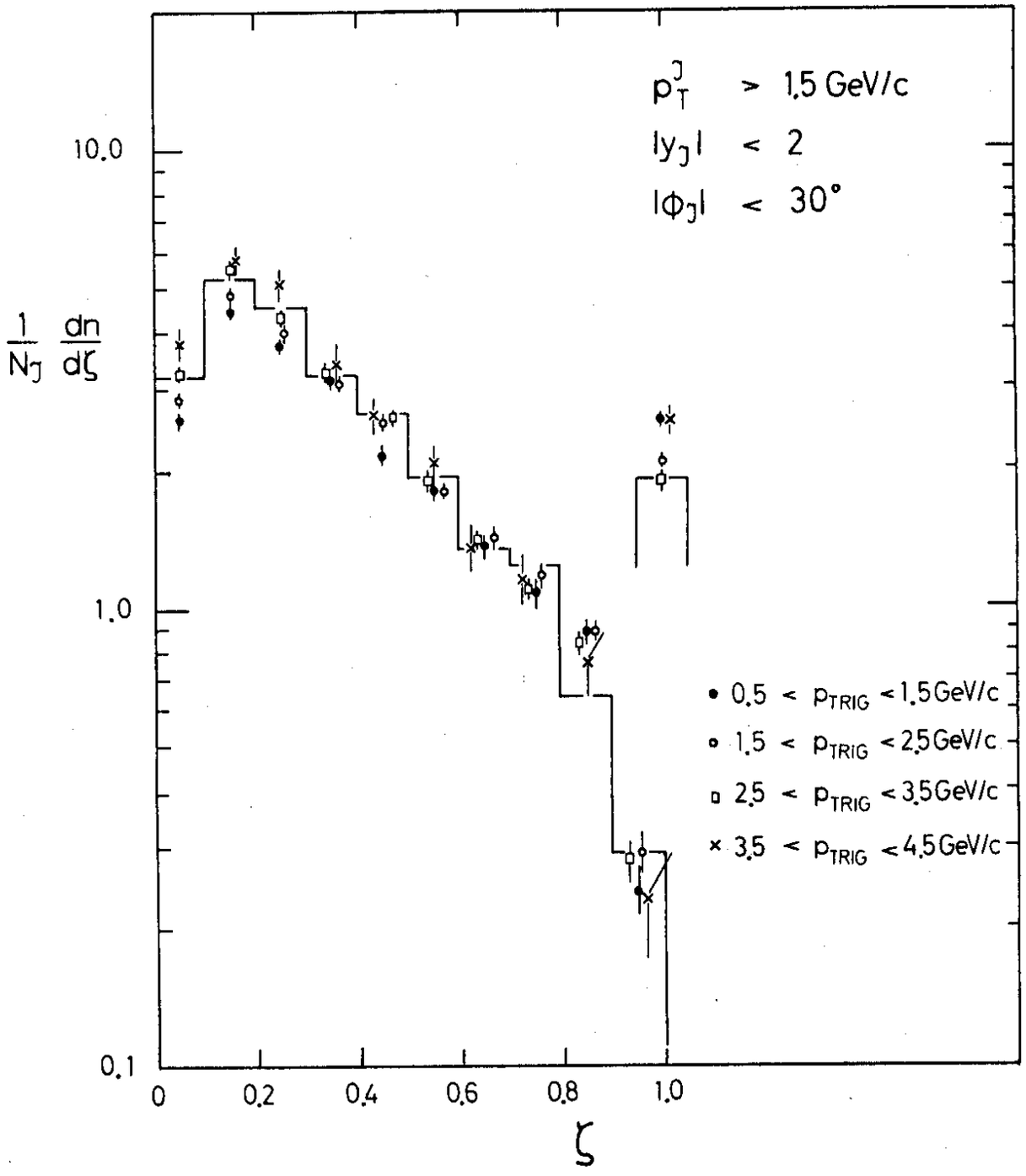
p_T^J > 1.5 GeV/c
$|y_J|$ < 2
$|\phi_J|$ < 30°
$\frac{1}{N_J}\frac{dn}{d\zeta}$
10.0
1.0
0.1
0
0.2
0.4
0.6
0.8
1.0
ζ
• 0.5 < p_{TRIG} < 1.5 GeV/c
○ 1.5 < p_{TRIG} < 2.5 GeV/c
□ 2.5 < p_{TRIG} < 3.5 GeV/c
× 3.5 < p_{TRIG} < 4.5 GeV/c

Fig. 16

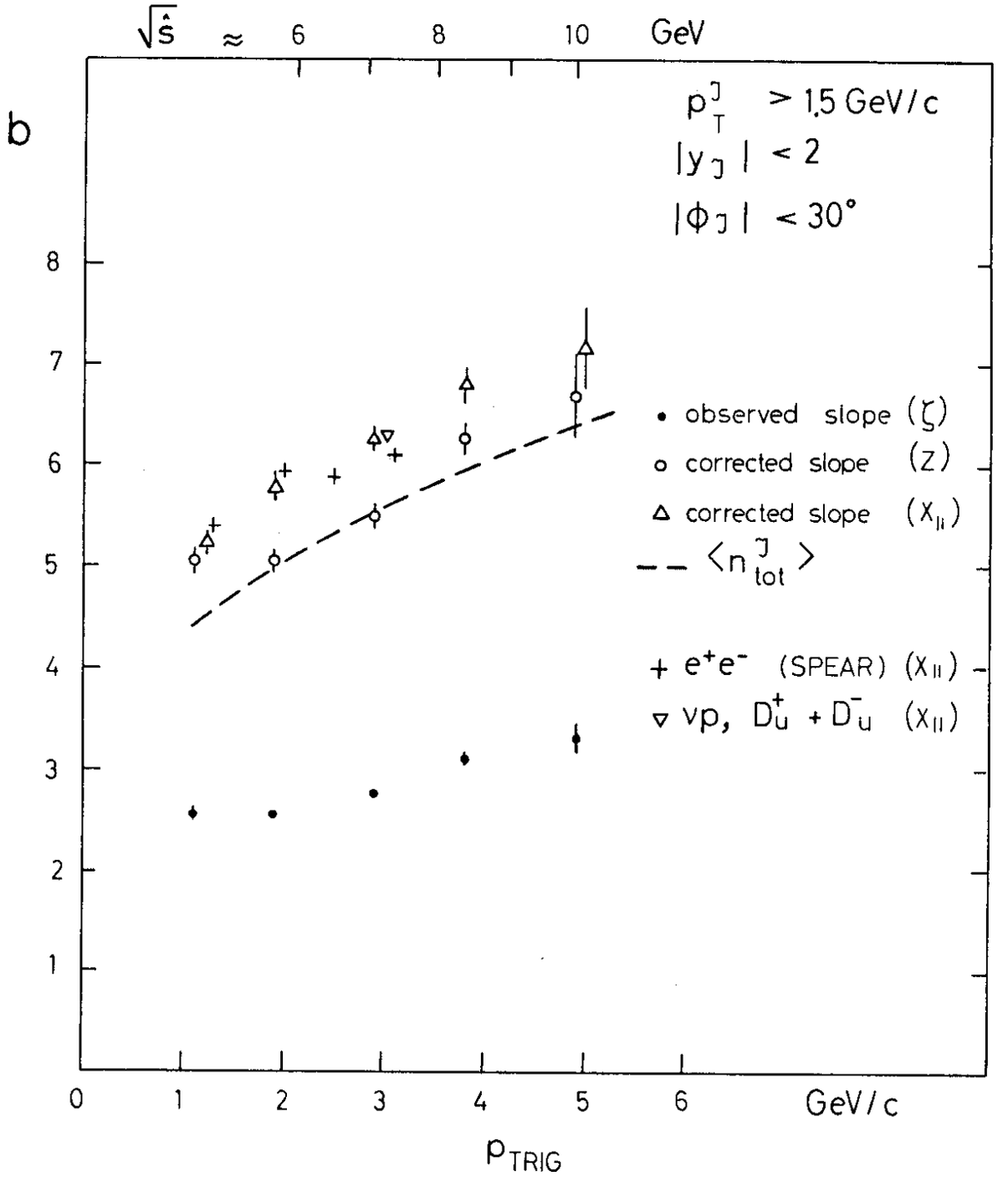
b
$\sqrt{\hat{s}}$ ≈ 6 8 10 GeV
p_T^J > 1.5 GeV/c
$|y_J|$ < 2
$|\phi_J|$ < 30°
• observed slope (ζ)
o corrected slope (Z)
Δ corrected slope ($X_{||}$)
-- $\langle n_{tot}^J \rangle$
+ e^+e^- (SPEAR) ($X_{||}$)
▽ νp, $D_u^+ + D_u^-$ ($X_{||}$)
0 1 2 3 4 5 6 GeV/c
p_{TRIG}
1 2 3 4 5 6 7 8

Fig. 17

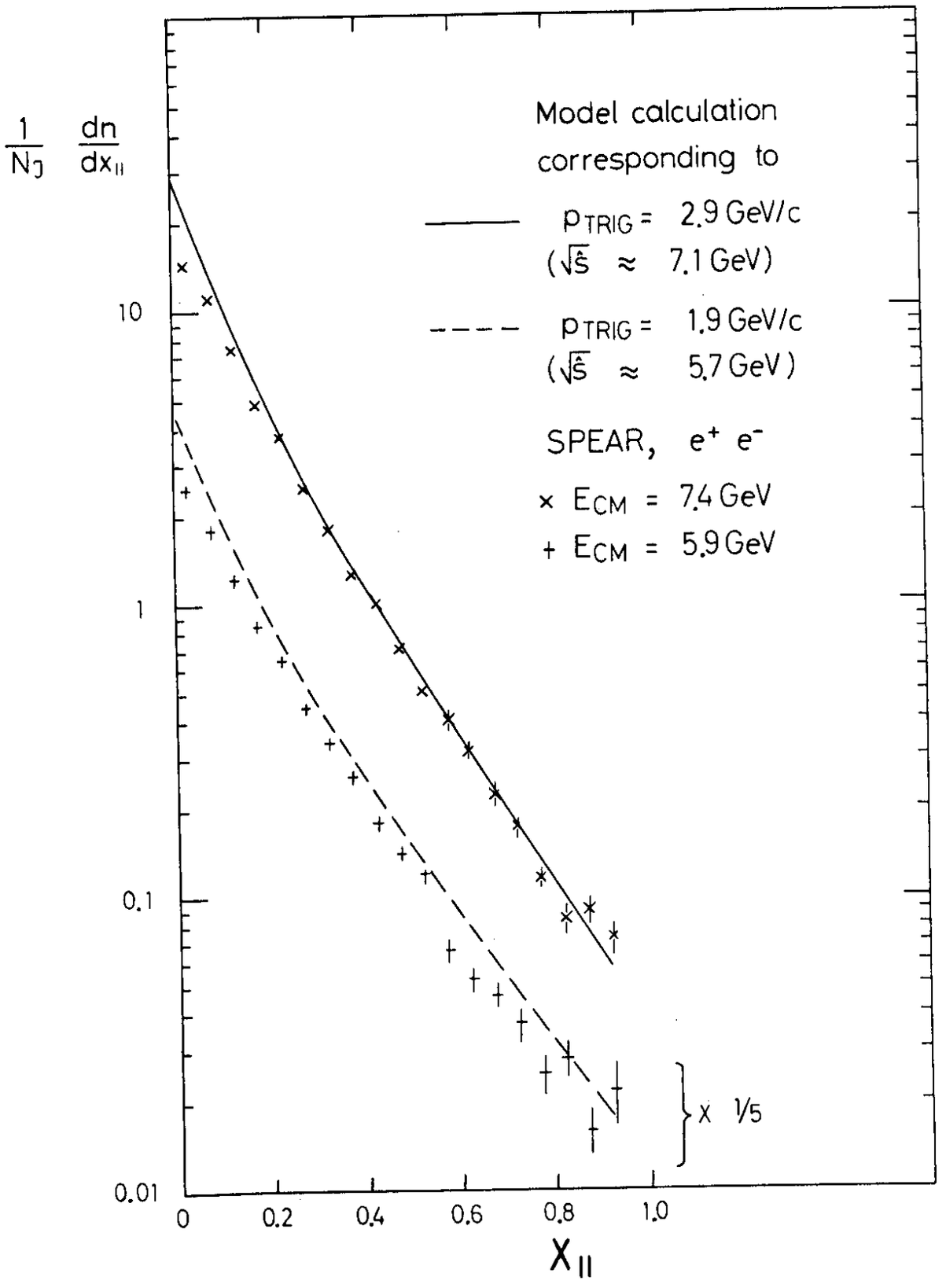
1/N_J dn/dx_II
Model calculation
corresponding to
p_TRIG = 2.9 GeV/c
(√ŝ ≈ 7.1 GeV)
p_TRIG = 1.9 GeV/c
(√ŝ ≈ 5.7 GeV)
SPEAR, e+ e-
× E_CM = 7.4 GeV
+ E_CM = 5.9 GeV
× 1/5
10
1
0.1
0.01
0
0.2
0.4
0.6
0.8
1.0
X_II

Fig. 18

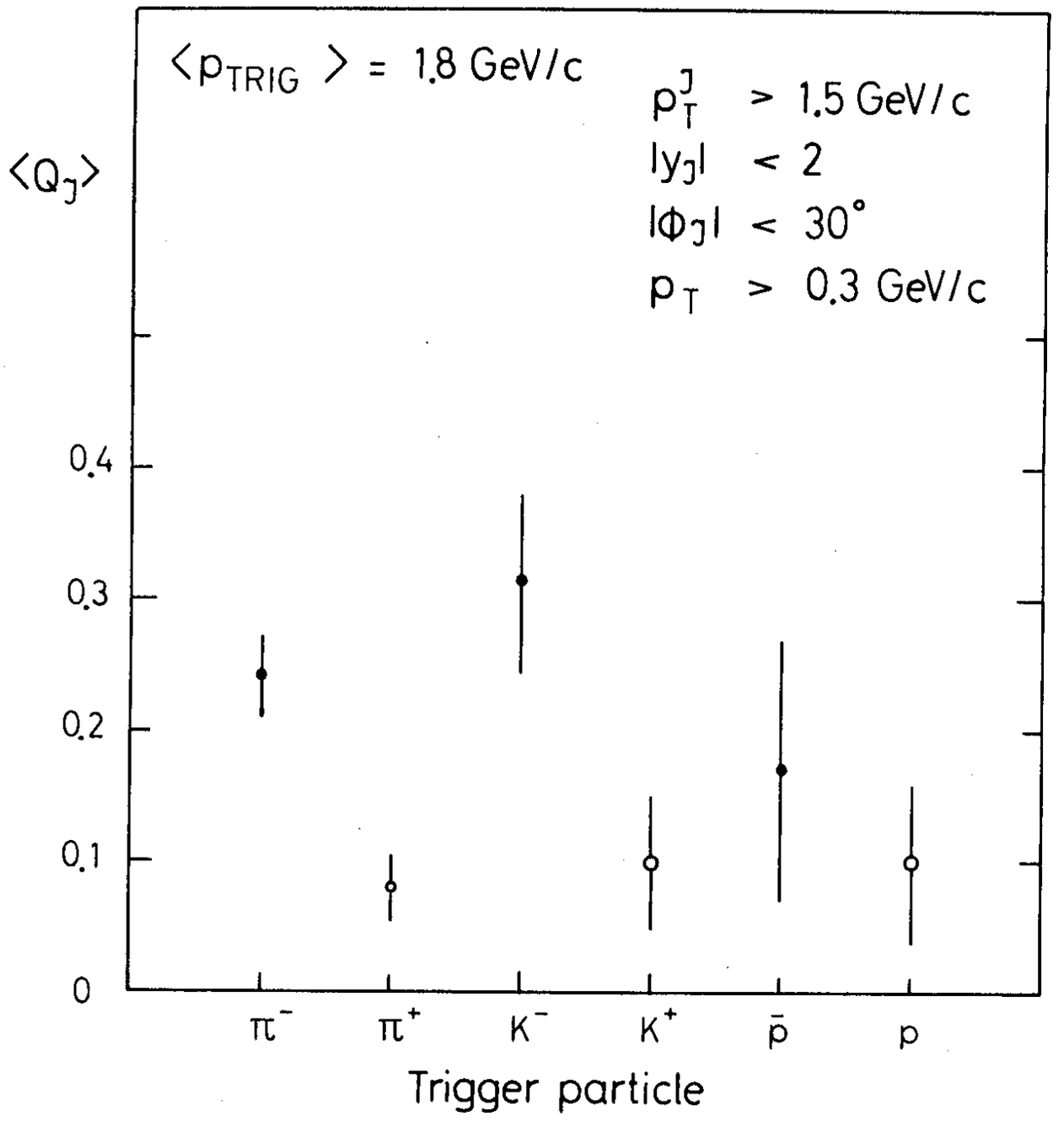
⟨pTRIG⟩ = 1.8 GeV/c
p_T^J > 1.5 GeV/c
|yJ| < 2
|ΦJ| < 30°
pT > 0.3 GeV/c
⟨QJ⟩
0.4
0.3
0.2
0.1
0
π⁻
π⁺
K⁻
K⁺
p̄
p
Trigger particle

Fig. 19

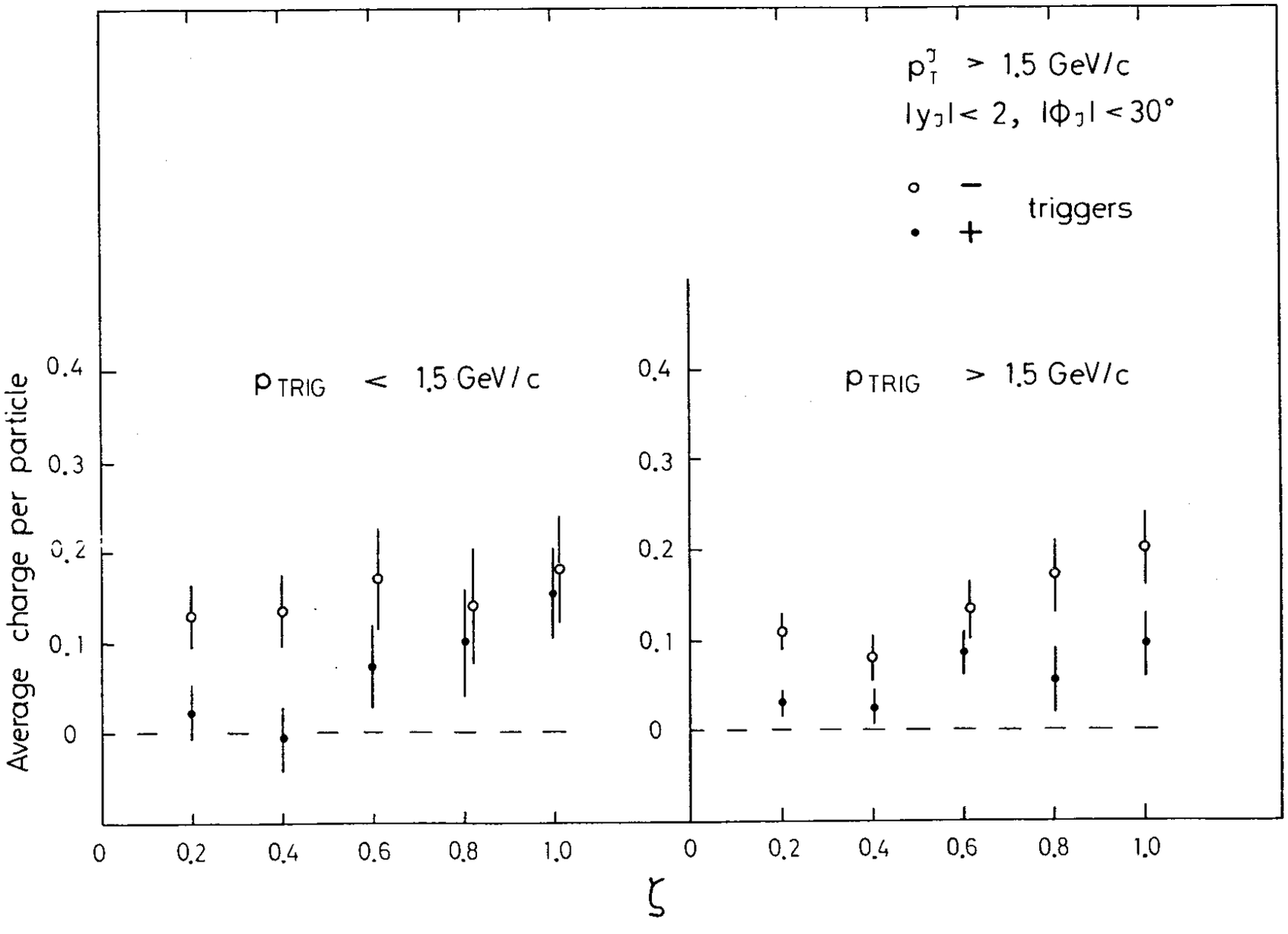
p_T^J > 1.5 GeV/c
$|y_J| < 2$, $|\phi_J| < 30°$
triggers
p_{TRIG} < 1.5 GeV/c
p_{TRIG} > 1.5 GeV/c
Average charge per particle
0.4
0.3
0.2
0.1
0
0.2
0.4
0.6
0.8
1.0
ζ

Fig. 20

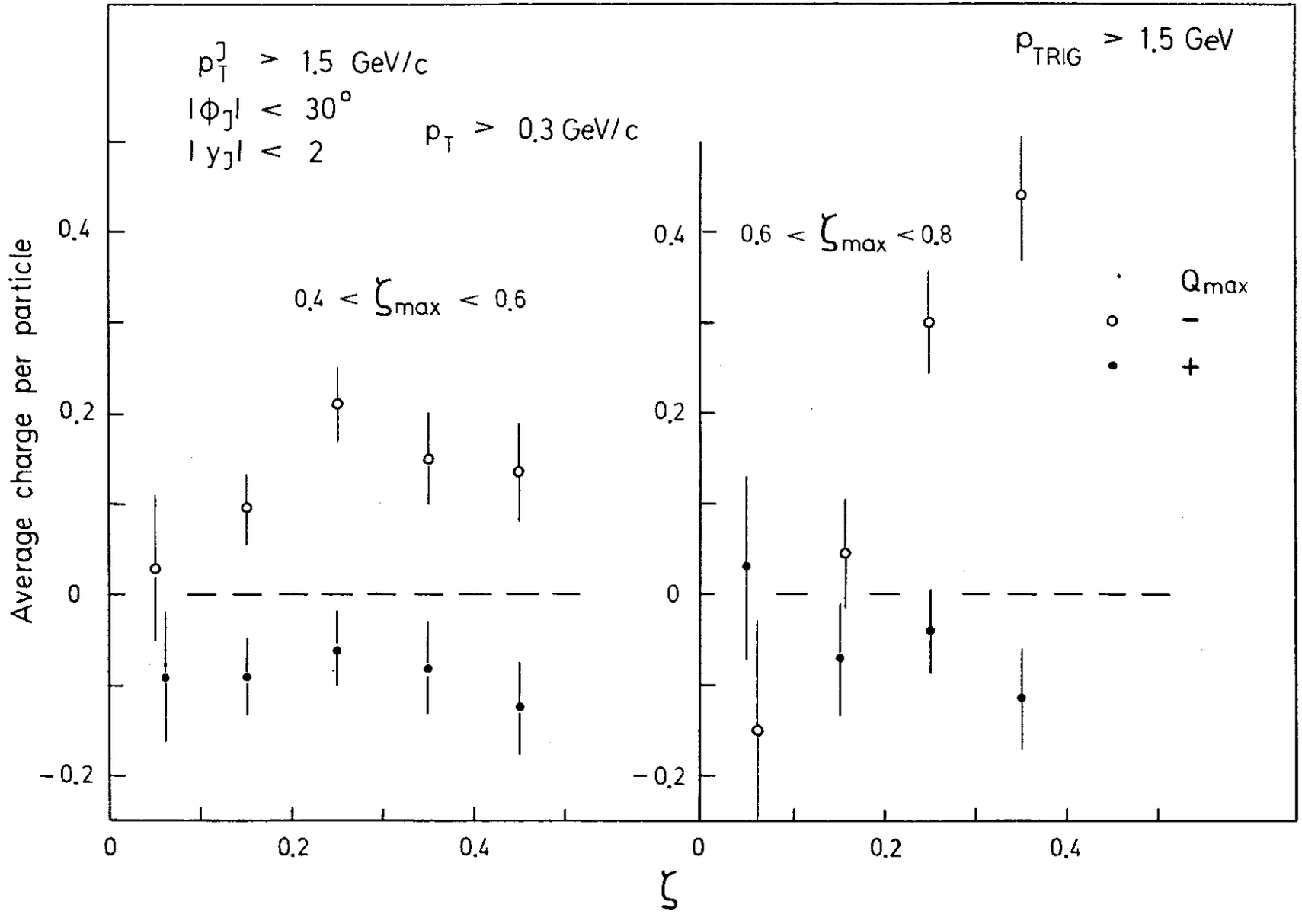
p_T^J > 1.5 GeV/c
$|\phi_J|$ < 30°
$|y_J|$ < 2
p_T > 0.3 GeV/c
p_{TRIG} > 1.5 GeV
0.4 < ζ_{max} < 0.6
0.6 < ζ_{max} < 0.8
Q_{max}
−
+
Average charge per particle
0.4
0.2
0
−0.2
0
0.2
0.4
ζ

Fig. 21

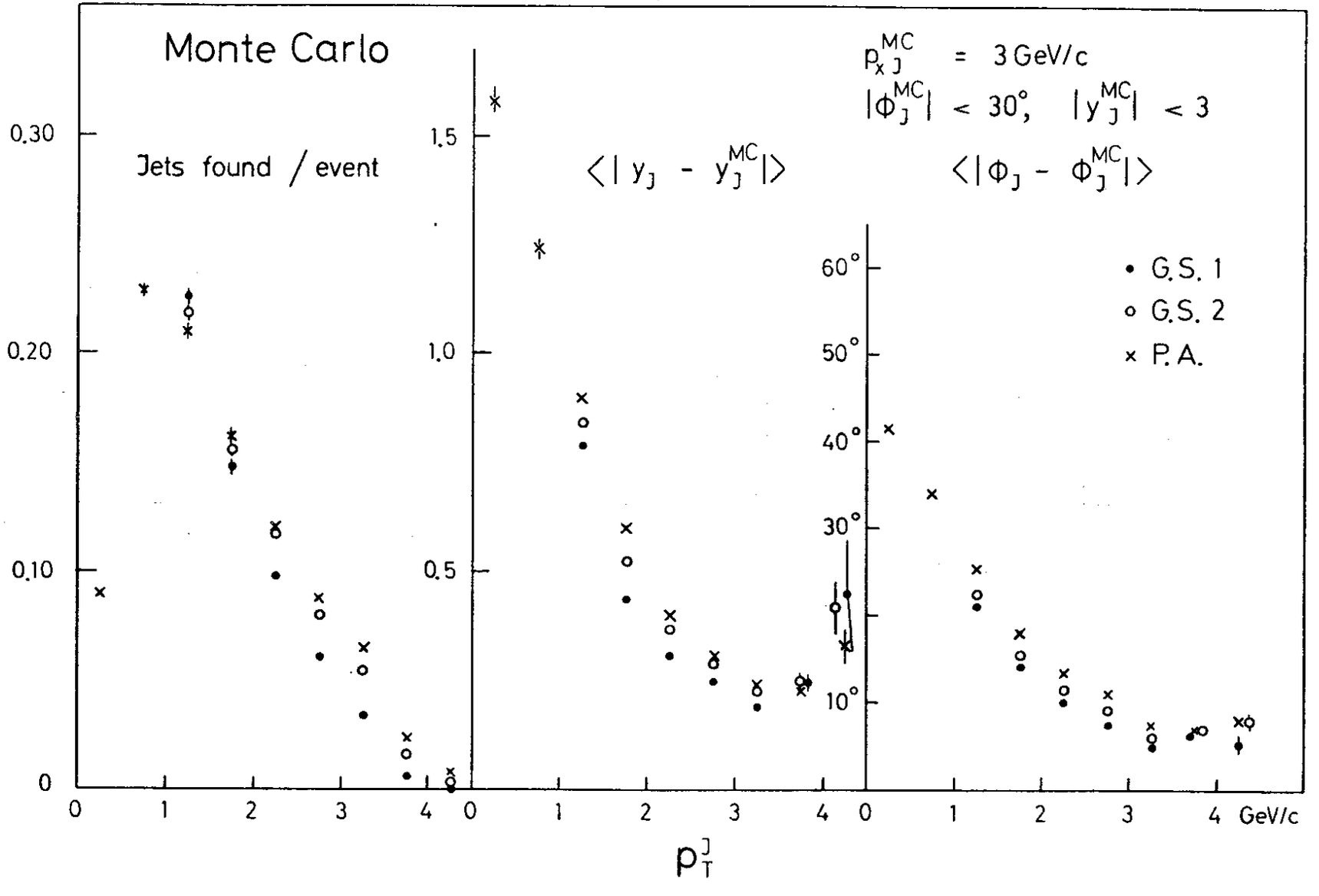
Monte Carlo
$p_{x\,J}^{MC}$ = 3 GeV/c
$|\Phi_J^{MC}| < 30°$, $|y_J^{MC}| < 3$
Jets found / event
$\langle |y_J - y_J^{MC}| \rangle$
$\langle |\Phi_J - \Phi_J^{MC}| \rangle$
G.S. 1
G.S. 2
P.A.
0.30
0.20
0.10
0
1.5
1.0
0.5
60°
50°
40°
30°
10°
0 1 2 3 4 GeV/c
p_T^J

Fig. B1

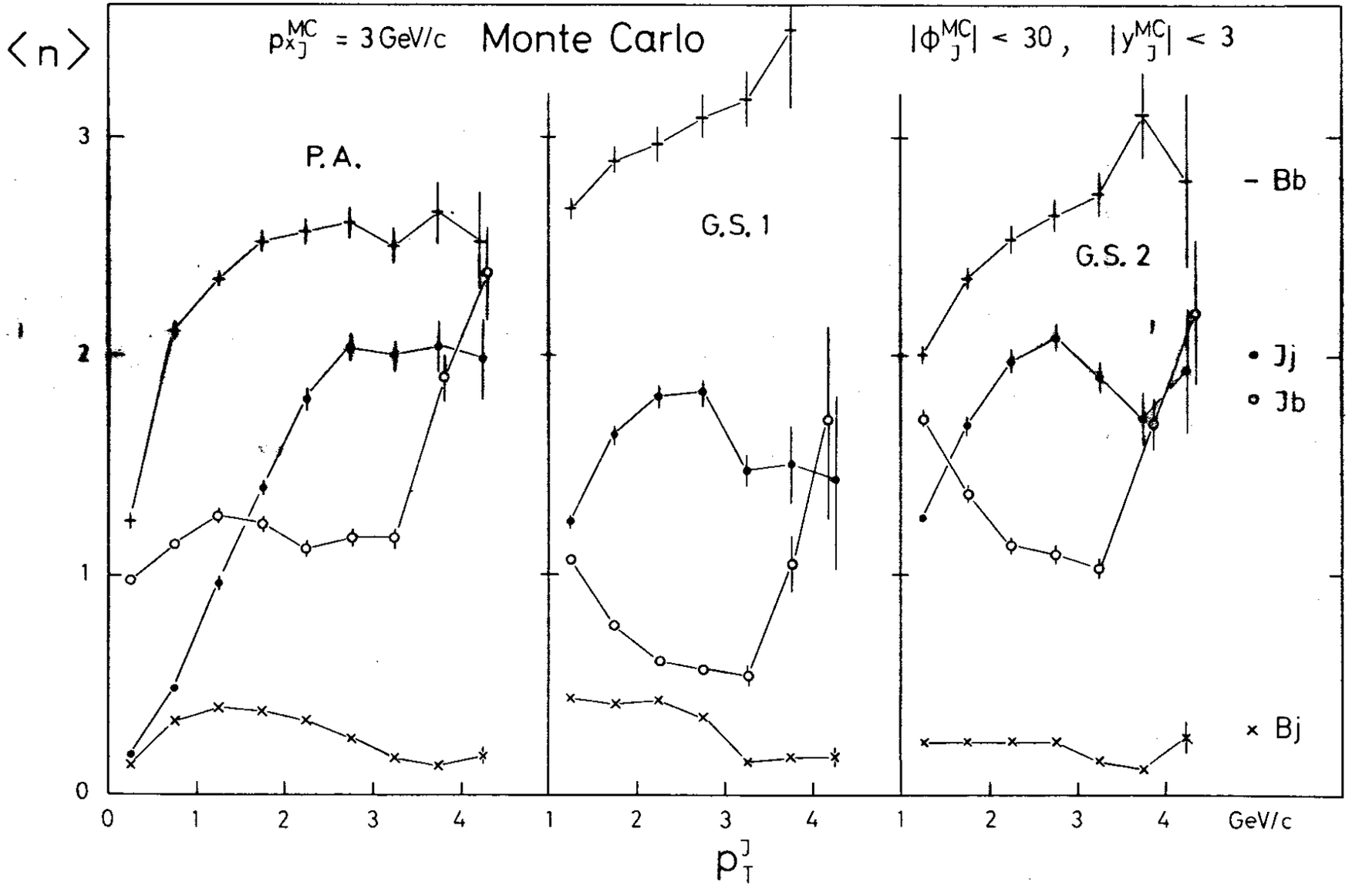
⟨n⟩
$p_{x_J}^{MC}$ = 3 GeV/c Monte Carlo
$|\phi_J^{MC}| < 30$, $|y_J^{MC}| < 3$
P.A.
G.S. 1
G.S. 2
- Bb
• Jj
○ Jb
× Bj
0
1
2
3
4
GeV/c
p_T^J

Fig. B2

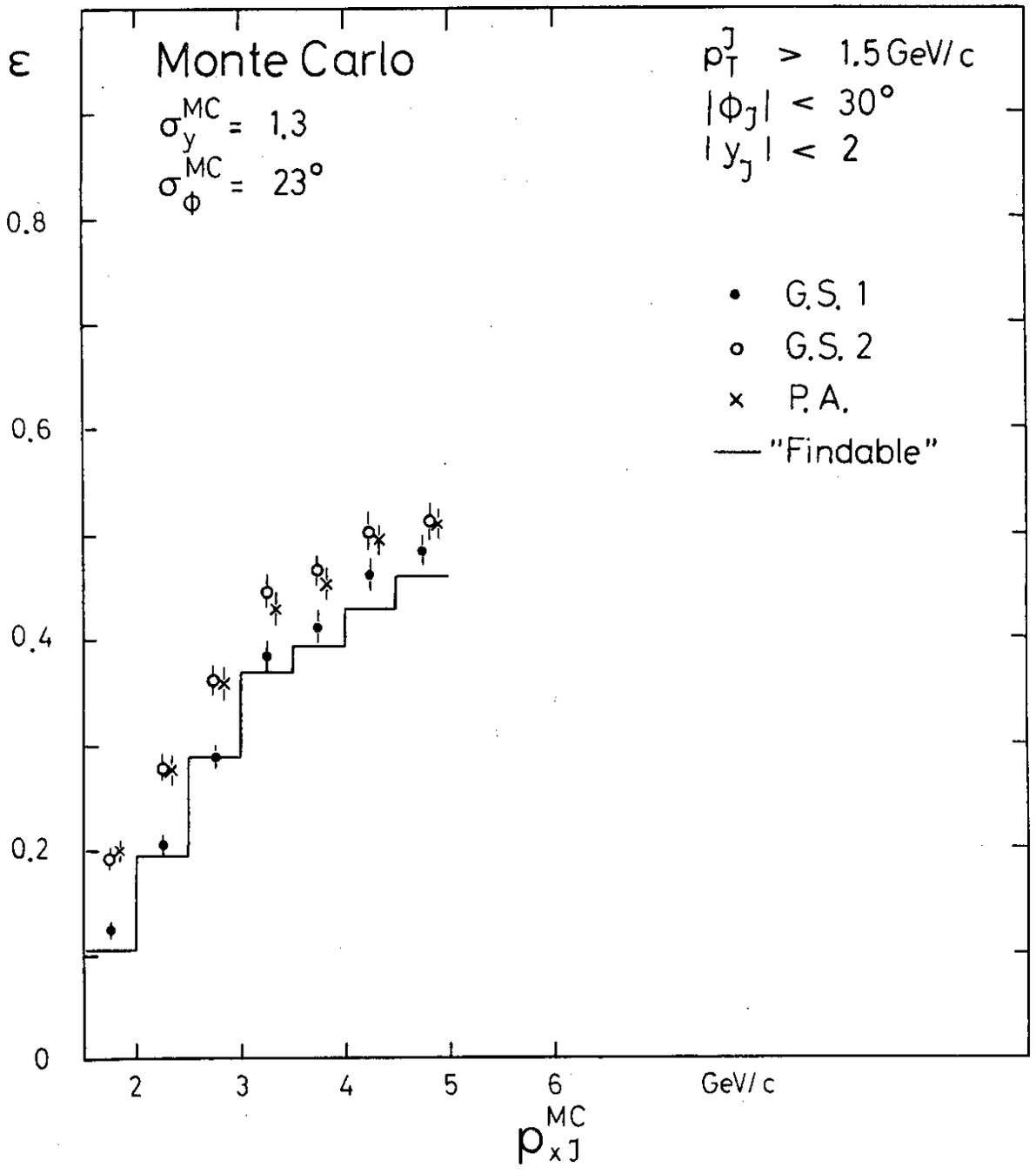
ε
Monte Carlo
σ_y^{MC} = 1.3
σ_ϕ^{MC} = 23°
p_T^J > 1.5 GeV/c
$|\phi_J|$ < 30°
$|y_J|$ < 2
G.S. 1
G.S. 2
P.A.
"Findable"
0.8
0.6
0.4
0.2
0
2
3
4
5
6
GeV/c
p_{xJ}^{MC}

Fig. B3

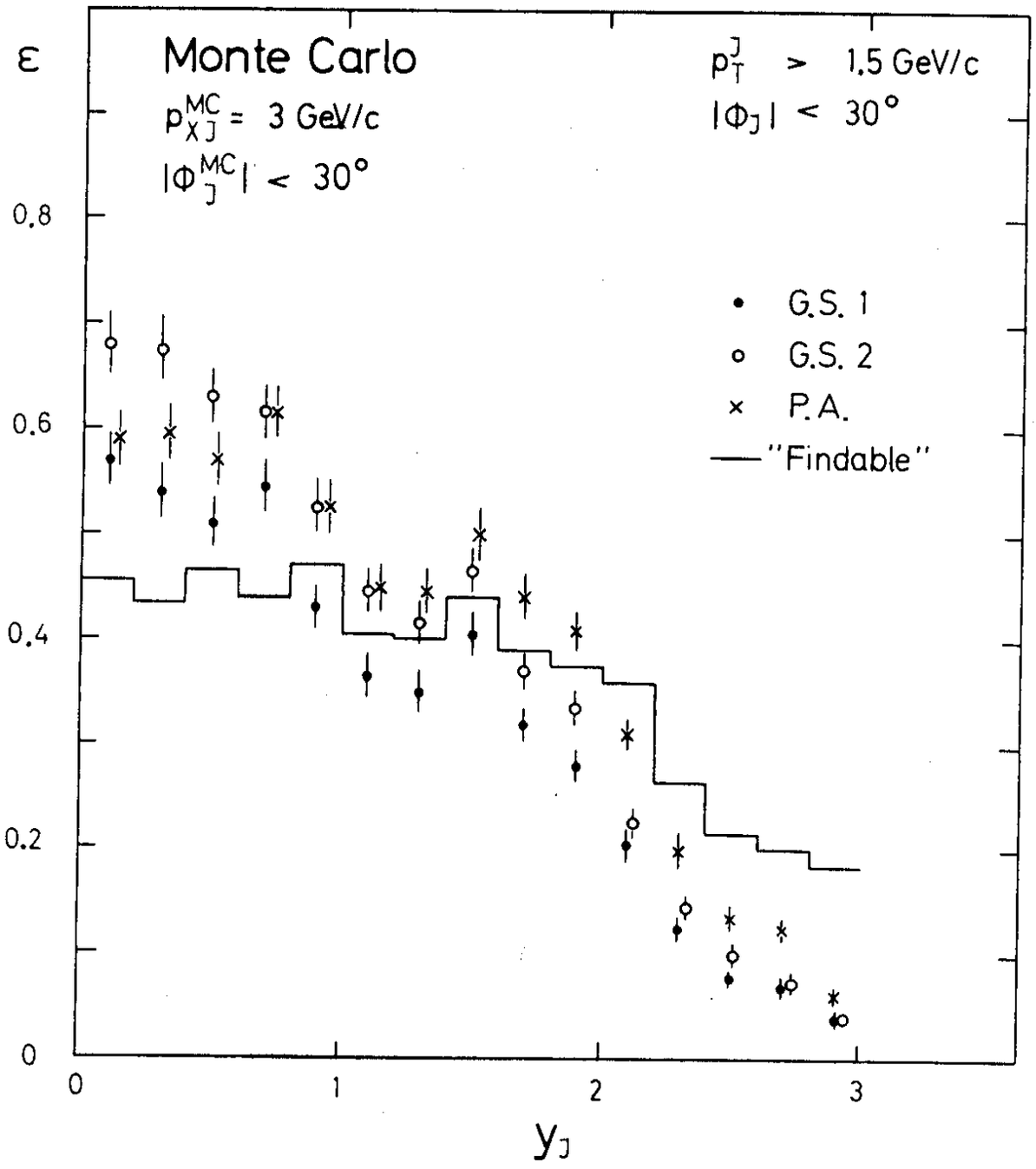
ε
Monte Carlo
p_{XJ}^{MC} = 3 GeV/c
$|\Phi_J^{MC}| < 30°$
$p_T^J > 1.5$ GeV/c
$|\Phi_J| < 30°$
G.S. 1
G.S. 2
P.A.
"Findable"
0.8
0.6
0.4
0.2
0
0
1
2
3
y_J

Fig. B4

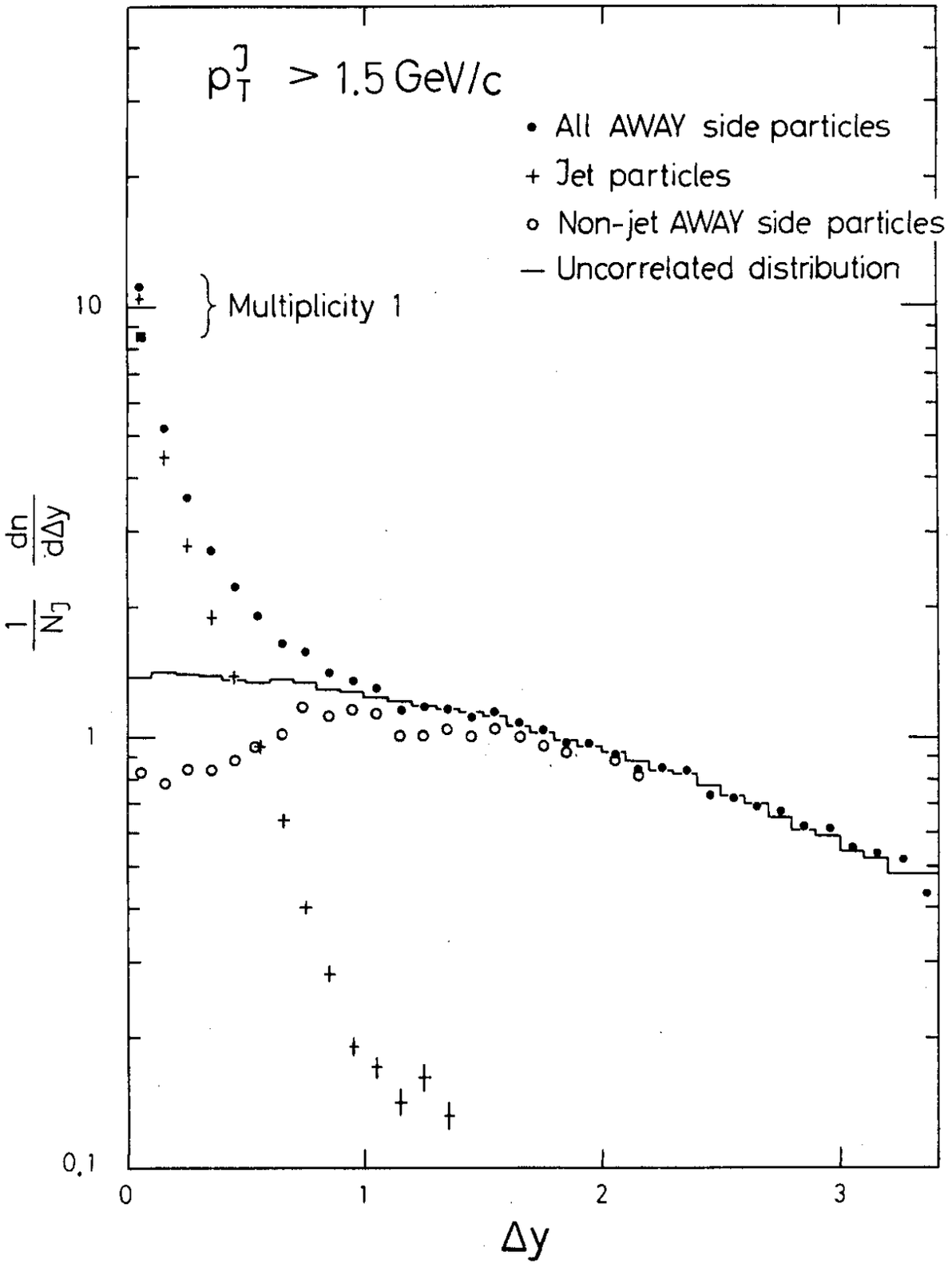
$p_T^J > 1.5$ GeV/c
• All AWAY side particles
+ Jet particles
o Non-jet AWAY side particles
— Uncorrelated distribution
Multiplicity 1
10
1
0.1
$\frac{1}{N_J}\frac{dn}{d\Delta y}$
0
1
2
3
Δy

Fig. B5